AEDC-TR-74-128

WIND TUNNEL MODEL DEFORMATION MEASURING SYSTEM

Leonard Bogdan, R. F. Drzewiecki, and
G. R. Duryea
Calspan Corporation
Buffalo, New York 14221

February 1975

Final Report for Period July 6, 1974 – August 1, 1974

Approved for public release; distribution unlimited.

Prepared for

DIRECTORATE OF TECHNOLOGY
ARNOLD ENGINEERING DEVELOPMENT CENTER
ARNOLD AIR FORCE STATION, TENNESSEE 37389

NOTICES

When U. S. Government drawings specifications, or other data are used for any purpose other than a definitely related Government procurement operation, the Government thereby incurs no responsibility nor any obligation whatsoever, and the fact that the Government may have formulated, furnished, or in any way supplied the said drawings, specifications, or other data, is not to be regarded by implication or otherwise, or in any manner licensing the holder or any other person or corporation, or conveying any rights or permission to manufacture, use, or sell any patented invention that may in any way be related thereto.

Qualified users may obtain copies of this report from the Defense Documentation Center.

References to named commercial products in this report are not to be considered in any sense as an endorsement of the product by the United States Air Force or the Government.

This final report was submitted by Calspan Corporation, Buffalo, New York 14221, under contract F40600-73-C-008, with the Directorate of Technology, Arnold Engineering Development Center (AEDC), Air Force Systems Command (AFSC), Arnold Air Force Station, Tennessee 37389. First Lieutenant Keith L. Kushman, Directorate of Technology, AEDC, was the Project Engineer/Scientist-in-Charge.

This report has been reviewed by the Information Office (OI) and is releasable to the National Technical Information Service (NTIS). At NTIS, it will be available to the general public, including foreign nations.

APPROVAL STATEMENT

This technical report has been reviewed and is approved for publication.

FOR THE COMMANDER

Keith L. Kushman

KEITH L. KUSHMAN
First Lieutenant, USAF
Research and Development
Division
Directorate of Technology

Robert O Dietz

ROBERT O. DIETZ
Director of Technology

REPORT DOCUMENTATION PAGE		READ INSTRUCTIONS BEFORE COMPLETING FORM
1. REPORT NUMBER AEDC-TR-74-128	2. GOVT ACCESSION NO.	3. RECIPIENT'S CATALOG NUMBER
4. TITLE *(and Subtitle)* WIND TUNNEL MODEL DEFORMATION MEASURING SYSTEM		5. TYPE OF REPORT & PERIOD COVERED Final Report - July 6, 1973 - August 1, 1974 6. PERFORMING ORG. REPORT NUMBER RK-5345-A-1
7. AUTHOR(s) L. Bogdan, R. F. Drzewiecki, and G. R. Duryea, Calspan Corporation Buffalo, New York 14221		8. CONTRACT OR GRANT NUMBER(s) F40600-73-C-0008
9. PERFORMING ORGANIZATION NAME AND ADDRESS Calspan Corporation Buffalo, New York 14221		10. PROGRAM ELEMENT, PROJECT, TASK AREA & WORK UNIT NUMBERS
11. CONTROLLING OFFICE NAME AND ADDRESS Arnold Engineering Development Center (DYFS) Arnold Air Force Station, Tennessee 37389		12. REPORT DATE February 1975 13. NUMBER OF PAGES 88
14. MONITORING AGENCY NAME & ADDRESS(*if different from Controlling Office*)		15. SECURITY CLASS. (*of this report*) UNCLASSIFIED 15a. DECLASSIFICATION/DOWNGRADING SCHEDULE N/A

16. DISTRIBUTION STATEMENT *(of this Report)*

Approved for public release; distribution unlimited.

17. DISTRIBUTION STATEMENT *(of the abstract entered in Block 20, if different from Report)*

18. SUPPLEMENTARY NOTES

Available in DDC

19. KEY WORDS *(Continue on reverse side if necessary and identify by block number)*

wind tunnel models
probes
wing deflections
wing twist
strain gages
pitch angle

20. ABSTRACT *(Continue on reverse side if necessary and identify by block number)*

This program was concerned with a feasibility study of an on-board type sensing technique capable of accurate measurement of the deformation of wind tunnel models undergoing test in the unique operational environment of the High Reynolds Number Wind Tunnel (HIRT). Analytical and experimental investigations were devoted to establishing the utility of a strain-gage probe type of sensor for the measurement of the deflection and twist

DD FORM 1 JAN 73 1473 EDITION OF 1 NOV 65 IS OBSOLETE

20. ABSTRACT (Continued)

occurring in model wings as the result of aerodynamic loading. Static-type tests of a prototype device were conducted and substantiated the analytical conclusions that the accuracy goals in wing deflection (0.05 inch) and wing twist angle (0.1 degree) could be achieved.

AFSC
Arnold AFS Tenn

PREFACE

The work reported herein was conducted by the Aerodynamic Research Department of Calspan Corporation, Buffalo, New York. The work was sponsored by the Arnold Engineering Development Center (AEDC), Air Force Systems Command (AFSC), Arnold Air Force Station, Tennessee, under Contract Number F40600-73-C-0008. The work was conducted during the period from July 1973 to August 1974. First Lieutenant Keith L. Kushman, Directorate of Technology, AEDC, was the Project Engineer/ Scientist-in-Charge. Mr. Ronald Drzewiecki was the Calspan Project Engineer.

The investigation of model pitch angle instrumentation was made by R. W. Huber, who also contributed Appendix D. R. J. Chmaj installed and wired the strain gages, and the electronic readouts were provided by A. J. LaPres. The computer programming was done under the cognizance of C. J. Reid, Jr.

The reproducibles used in the reproduction of this report were supplied by the authors.

TABLE OF CONTENTS

TABLE OF CONTENTS (Cont.)

LIST OF ILLUSTRATIONS

LIST OF TABLES

Section 1.0
INTRODUCTION

The Arnold Engineering and Development Center (AEDC) is planning to acquire a High Reynolds Number Wind Tunnel (HIRT) having the capability to duplicate the flight Reynolds number of large, high-performance aircraft and launch vehicles in the Mach number range from 0.2 to 1.4. The HIRT is to employ the Ludwieg tube concept and provide an 8 x 10 foot test section.

In achieving the high unit Reynolds numbers, the models will perforce be highly loaded during test. In response to these high loads, the model surfaces will deflect (bend and twist) relative to their unloaded shape. In consequence of the fact that small changes in model shape can have a significant effect on aerodynamic measurements, the need for continuous data on model deformation during a tunnel test run is essential.

AEDC has underway a design study of a model deformation measurement system based on the use of Moiré pattern techniques which offer the potential for determining continuous deformation data over the entire viewable surface of the model. Since the practical and economic aspects of this technique to the HIRT requirements remain to be established, the need for an alternate measurement technique, independent of optical methods, exists. One possible alternate technique would operate in a model coordinate system using sensors installed within the model and be capable of resolving local as well as gross model deflections. Such a system would provide real time model deformation data but only at selected locations on the model. This report describes studies, both analytical and experimental, undertaken for AEDC and directed towards a system design of a model deformation measuring system based on the use of strain-gage sensors.

Program effort was divided into two phases, an analytical phase and an experimental phase. In the initial phase, effort was devoted to the development of a practical concept of adapting strain gage sensors to the HIRT application with a view to satisfying stipulated performance requirements under the range of the environmental parameters encountered and the imposed spatial constraints of the models. Principal emphasis was placed on the measurement of wing deflection and wing twist. The main thrust of Phase I was the verification of the feasibility of the proposed concept by an analysis of the primary limitations of adapting the technique to the HIRT tunnel. Section 2.0 of the report presents the results of the Phase I study.

Phase II effort involved the experimental substantiation of the Phase I estimates of system performance. A prototype strain-gage beam and a mating, simulated wing section were fabricated, together with a test fixture. The purpose was to obtain test data establishing (1) the degree of agreement between wing deflection data computed from sensor output signals

and the directly measured deflections, (2) the effects of wing twist on the accuracy of probe-measured deflections and (3) the thermal effects on probe measurements. The results of Phase II are given in Section 3.0 of the report.

Section 2.0
PHASE I -- ANALYTICAL STUDIES

2.1 STUDY GUIDELINES

The guidelines laid down for the Phase I effort were detailed and explicit. In the interests of conciseness, the criteria specified by AEDC for the development of a self-contained sensor system for model deformation are itemized below:

- The measurement system shall provide real-time, continuous, local and gross model deformation data during a two and one-half second tunnel run (with consideration given to accommodating test times up to ten seconds).
- All sensors will be located within the model and require minimum space.
- The system will not interfere in any manner with the aerodynamic flow in the test section, require a minimum of access ports in the perforated test section walls and not compromise operation of the tunnel.
- Instrumentation mounted within the model must withstand ambient temperatures in the range from -60°F to +100°F and pressures to 800 psia including depressurization from 800 to 500 psia in one-half second (involved in normal tunnel operation).
- The system must be capable of sensing local model deflections up to 3 inches with a nominal accuracy of 0.05 inches and local twist angles up to 4 degrees with a nominal accuracy of 0.1 degree.
- The model will be pitched during a run over a -10 degree to +20 degree range at rates up to 7 degrees per second. Pitch angle will be sensed to a nominal accuracy of 0.1 degree.
- The system will provide an output suitable for recording for subsequent analysis.

To provide a specific focus for obtaining dimensional inputs in analyzing a specific system design, emphasis was to be placed on models with a high-aspect-ratio wing. A 1/24th scale model of the Advanced Technology Transport (ATT) was designated for this purpose.

2.2 PROBE CONCEPT

The strain gage system conceived for measuring model deformation satisfies all of the system requirements cited in Section 2.1 above with the sole exception of an ability to sense gross model motion (pitch angle, whose measurement by alternate methods is discussed in Section 2.8). This system incorporates strain gage probes mounted in the model wing in a spanwise direction. Each probe is essentially an instrumented spanwise cantilever beam fixed at the wing root and constrained by a number of moment-free connections through which the wing loads are transmitted. These connections deflect the beam in a direction normal to wing chord plane by an amount equal to the wing deflection at these points. Strain gage bridges, equal in number to the number of load connection points, are so disposed as to produce electrical outputs in response to deflections at the load points.

It is possible to envision a single probe so instrumented that it could simultaneously measure wing deflection and wing twist. Practical considerations led to the conclusion that such a probe would be very difficult to implement within the size constraints imposed. For example, a consideration of the typical wing chord thickness of the ATT model coupled with a need for the probe to extend to about three-quarters of the wing semi-span dictated a probe outer diameter of about 0.3 inch maximum. Attempts to design suitable flexures as moment-free connections between the beam and wing proved to be unsuccessful even for a simple deflection probe because of spatial problems. Consequently, a dual probe geometry was selected to provide measurement of both wing bending and twist. Figure 1 illustrates the dual probe geometry whereby the wing twist angle in radians is equal to the chordwise differential deflection between probe "A" and probe "B" divided by the chordwise separation between the probes (d_2 in the figure). The circled areas in the planform view indicate the moment-free connections which comprise miniature precision ball bearings carefully fitted to the bore to minimize bearing "play" or lost motion.

As seen from the figure, the probe technique only provides deflection data at discrete points. Discussions with AEDC personnel indicated that an interpolative approach, based on known wing bending shapes, would be used to generate continuous spanwise deflection and twist data. It was also agreed that three spanwise, discrete measurements would be sufficient for the needs of this program. Principally for ease of mathematical analysis, the three reaction points were always taken to be uniformly spaced along the beam.

The inherent simplicity of using strain gages for measurement purposes contributes to the attractiveness of this technique for measuring model deformation. Unlike the situation with such other techniques as the optical Moiré pattern method, the probe electrical output is directly related to deflection. The need for complex data reduction procedures and other peripheral equipment is thus obviated. Further, wind tunnel personnel have long been familiar with strain-gage balance systems so that the assimilation of the strain gage probe into the family of wind tunnel instruments should be accomplished with ease.

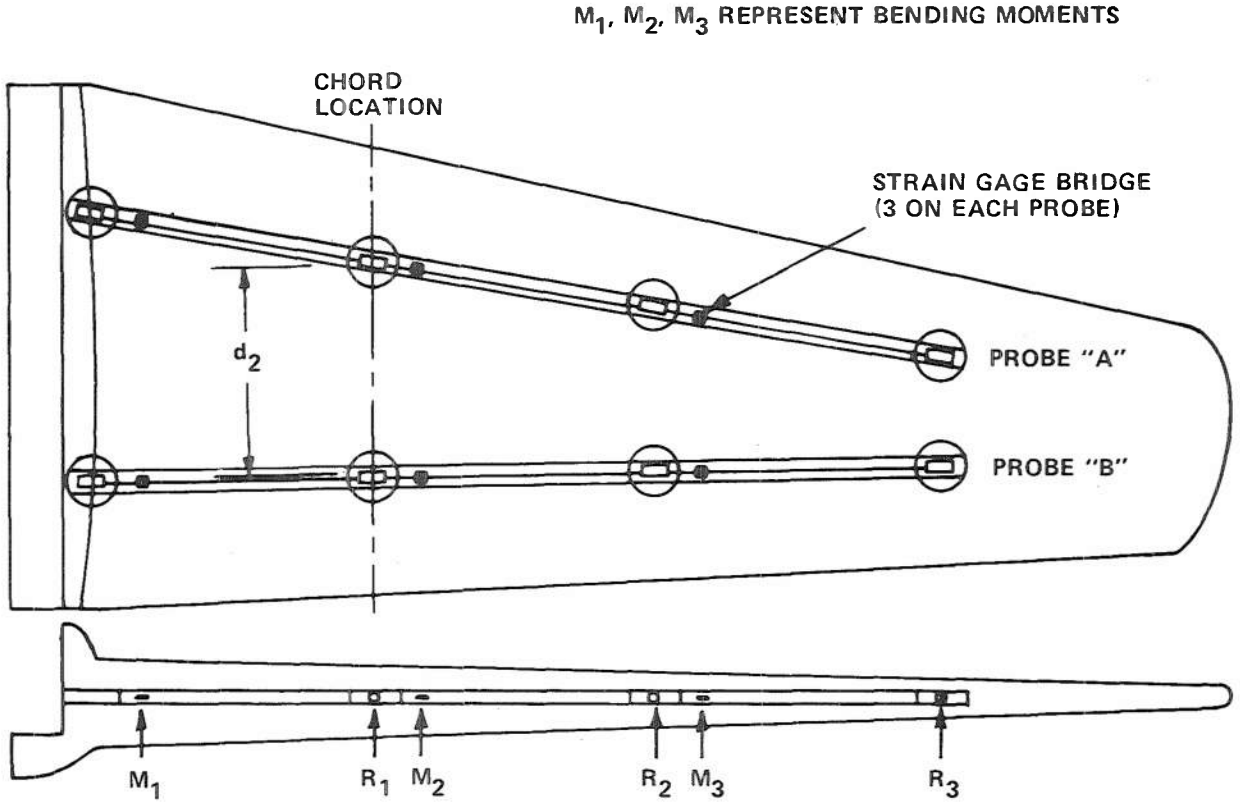

Figure 1 DUAL PROBE GEOMETRY (TYPICAL)

2.3 LITERATURE SURVEY

At the behest of AEDC personnel, a brief literature survey was conducted to fulfill two objectives: first, to do a state-of-the-art survey of strain gage technology with specific reference to the HIRT application of the strain gage probe, and second, to ascertain if the technical literature documented any prior uses of strain gage techniques for model deformation measurement.

The details of the strain gage technology study are not essential to the development of the body of this report and are therefore presented in Appendix A. It will suffice here to discuss only certain salient features of the bonded-type resistance strain gage which experiences resistance changes as the surface to which it is attached is subjected to strains. Specific attributes which make the strain gage such a useful sensor are itemized below.

- small size
- light weight and ruggedness
- ease of attachment and mounting
- low cost
- excellent electrical stability
- low impedance
- usable with a-c or d-c excitation
- operable over wide temperature extremes
- very high frequency response for dynamic studies

A low inherent sensitivity characterizes the metal strain gage; however, simple but sensitive electrical circuits are available to offset this factor.

The two principal types of gages in use today are the metal foil gage and the semiconductor gage. Metal foil gages are fabricated using photoetching techniques and feature extremely thin, flat ribbon-type conductors which facilitate excellent adhesion with good heat dissipation. The fabrication technique permits the gage to be executed in very small sizes and very complex shapes and patterns. Semiconductor strain gages are fabricated from grown silicon crystals doped with controlled impurity to achieve desired electrical properties. While these gages share some of the characteristics of the metal foil gage, their main attribute is a high sensitivity, as much as one hundred times that of the foil gage. On the other hand, the semiconductor gage is susceptible to large temperature effects and a nonlinear input-output characteristic. Metal foil gages are almost always preferred unless the high sensitivity of the semiconductor gage is crucial in a given application.

Strain gages may be employed in a variety of electrical circuit configurations. In general, a bridge-type circuit comprised of four active

gages* is most often used because of its increased sensitivity over other configurations (using fewer gages), linearity of output and inherent self-compensation of certain thermal effects.

The substance of the survey showed that strain gages are entirely adequate in accommodating the environmental requirements of the HIRT application.

A brief search for pertinent technical literature concerned with past experience in the use of strain-gage instrumentation for wind tunnel model deformation measurements was not productive. Calspan Transonic Tunnel personnel provided a contact with an aerodynamic test engineer at General-Dynamics (G-D) at Forth Worth, Texas(1). G-D was stated to have had limited experience in this area of endeavor and tests on a 1/15th scale F-111 were cited as an example. This model was instrumented with strain gages only in the wing-root area on the assumption that the model wing flexed like the full scale wing on the aircraft. No unusual application or operational difficulties were reported and a favorable disposition toward strain-gage sensing was expressed. G-D was not aware of the existence of any open literature on model deformation measurements.

2.4 MATHEMATICAL ANALYSIS

2.4.1 Parametric Relationships

This section is devoted to establishing the functional relationships among such parameters of the strain gage probe as bending moment, M, reaction load, R, and beam deflection, y.

Consider a three-segment, uniform cantilever beam of square cross-section and fixed at one end. Figure 2 illustrates such a configuration and designates the three locations along the beam length at which the reaction loads are applied as well as the three locations where the moments are determinable with strain gages. If the reaction points and the fixed end are separated by equal distances, ℓ, and the strain gages are located a distance "x" from the respective reactions, the moments may be expressed (in matrix form) as a function of the reactions

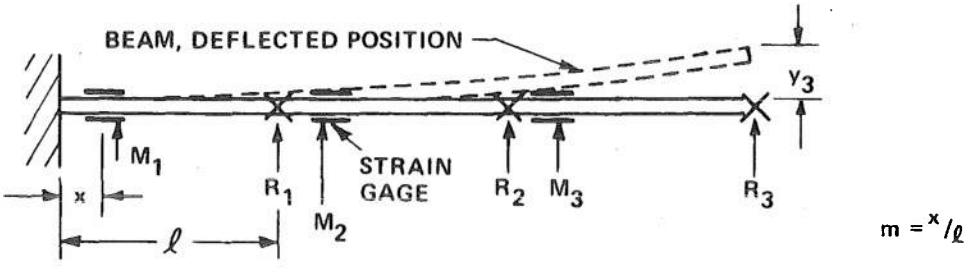

Figure 2 STRAIN GAGE PROBE REPRESENTATION

*These gages are connected electrically in such a manner that adjacent gages of the circuit experience strains of unlike polarity.

(1) Telecon, Mr. J. Schlicher, General Dynamics Corporation, Ft Worth, Texas, 6 August 1973.

$$\begin{bmatrix} M_1 \\ M_2 \\ M_3 \end{bmatrix} = \ell \begin{bmatrix} 1-m & 2-m & 3-m \\ 0 & 1-m & 2-m \\ 0 & 0 & 1-m \end{bmatrix} \begin{bmatrix} R_1 \\ R_2 \\ R_3 \end{bmatrix} \tag{1}$$

where $m = x/\ell$.

Beam deflections y_1, y_2, y_3 are expressible in terms of the reactions

$$\begin{bmatrix} y_1 \\ y_2 \\ y_3 \end{bmatrix} = \frac{\ell^3}{6EI} \begin{bmatrix} 2 & 5 & 8 \\ 5 & 16 & 28 \\ 8 & 28 & 54 \end{bmatrix} \begin{bmatrix} R_1 \\ R_2 \\ R_3 \end{bmatrix} \tag{2}$$

where EI is the flexural stiffness. Equations (1) and (2) may be combined to obtain the deflections as a function of the applied moments.

$$\begin{bmatrix} y_1 \\ y_2 \\ y_3 \end{bmatrix} = \frac{\ell^2}{6EI(1-m)^3} \begin{bmatrix} 2(1-m)^2 & (1-m)(1-3m) & -m(1-3m) \\ 5(1-m)^2 & (1-m)(6-11m) & (1-2m)(1-6m) \\ 8(1-m)^2 & 4(1-m)(3-5m) & 2(3-12m+13m^2) \end{bmatrix} \begin{bmatrix} M_1 \\ M_2 \\ M_3 \end{bmatrix} \tag{3}$$

Since the strain gage is directly responsive to strain rather than bending moment it is useful to express the deflections in terms of the strains.

$$\begin{bmatrix} y_1 \\ y_2 \\ y_3 \end{bmatrix} = \frac{\ell^2}{6\mathcal{Y}(1-m)^3} \begin{bmatrix} 2(1-m)^2 & (1-m)(1-3m) & -m(1-3m) \\ 5(1-m)^2 & (1-m)(6-11m) & (1-2m)(1-6m) \\ 8(1-m)^2 & 4(1-m)(3-5m) & 2(3-12m+13m^2) \end{bmatrix} \begin{bmatrix} \epsilon_1 \\ \epsilon_2 \\ \epsilon_3 \end{bmatrix} \tag{4}$$

where $\mathcal{Y}$ is one-half the beam thickness while ϵ is the strain.

The foregoing expressions provide the basis for understanding and optimizing the characteristics of the beam as a deflection sensor. Expected accuracies and the magnitude of the output response may be calculated by substituting assumed numerical data into these equations.

2.4.2 Accuracy Implications

As cited in preceding sections of this report, the strain gage probe technique will use a pair of probes, displaced chordwise along the wing. The dual probe configuration is required to permit twist angle measurement. While the measurement accuracies have been specified, nevertheless it is necessary to determine which of these specifications (0.05 inch in deflection or 0.1 degree in twist) is the critical factor for the dual-probe configuration.

With a 3/4 semi-span coverage with the probe required, a probe bore diameter of approximately 0.3 inch is determined from model wing thickness considerations. For the ATT model, it was established that the maximum probe separation distance, d, at 3/4 semi-span for this probe diameter is approximately 3 inches.

Wing deflection and wing twist data for the ATT model are graphically shown in Figures 3 and 4(2). Since the 3/4 semi-span of the ATT model corresponds to a length of 24 inches (approximately), the value of the probe parameter "ℓ" thus is equal to 8 inches. Taking the maximum deflection situation (2.5 g maneuver, 65% wing) the deflections and twist angles at the three (equally spaced) reaction points of the beam are as follows

$$y_1 = 0.036 \text{ inch}, \qquad \theta_1 = 0.3°$$

$$y_2 = 0.270 \text{ inch}, \qquad \theta_2 = 1.8°$$

$$y_3 = 2.000 \text{ inch}, \qquad \theta_3 = 3.5°$$

From the sketch of Figure 1 it is obvious that the following equation holds for the wing twist angle, θ

$$\sin \theta \cong \theta = \frac{y_a - y_b}{d} \tag{5}$$

where y_a and y_b are the deflections of probes A and B, respectively. The error equation is obtained by taking the total differential of equation (5) and assuming that the individual errors are random and combine as the square root of the sum of the squares.

Thus

$$\frac{\Delta\theta}{\theta} = \left[\left(\frac{y_a}{y_a - y_b}\right)^2\left(\frac{\Delta y_a}{y_a}\right)^2 + \left(\frac{y_b}{y_a - y_b}\right)^2\left(\frac{\Delta y_b}{y_b}\right)^2 + \left(\frac{\Delta d}{d}\right)^2\right]^{1/2} \tag{6}$$

where $y_a = y_3 + \frac{d\theta_3}{2}$, $y_b = y_3 - \frac{d\theta_3}{2}$*. Taking $y_3 = 2.00"$, $\theta_3 = 3.5°$ and assuming that accuracy in deflection measurement is ±1/4% and that $(\Delta d/d) \cong 0$, $\Delta\theta_3$ is calculated to be ≈ ±0.07° for d = 3 inches. Thus it is demonstrated that in the two-probe system it is the twist angle measurement that sets the numerical value for the accuracy of the deflection measurement.

To establish a more conservative goal in deflection measurement, an accuracy value of ±0.15% was selected which yields a $\Delta\theta_3$ value of ±0.04°. This accuracy is equivalent to a deflection tolerance of ±1.5 x 10^{-3} inches

*Thus $y_3 = \frac{y_a + y_b}{2}$

(2) Alexander, W.K., Griffin, S.A. et al., "Wing Tunnel Model Parametric Study for Use in the Proposed 8 ft x 10 ft High Reynolds Number Transonic Wind Tunnel (HIRT) at Arnold Engineering Development Center," General Dynamics Convair Aerospace Division, December 1972. AEDC-TR-73-47 (AD736725).

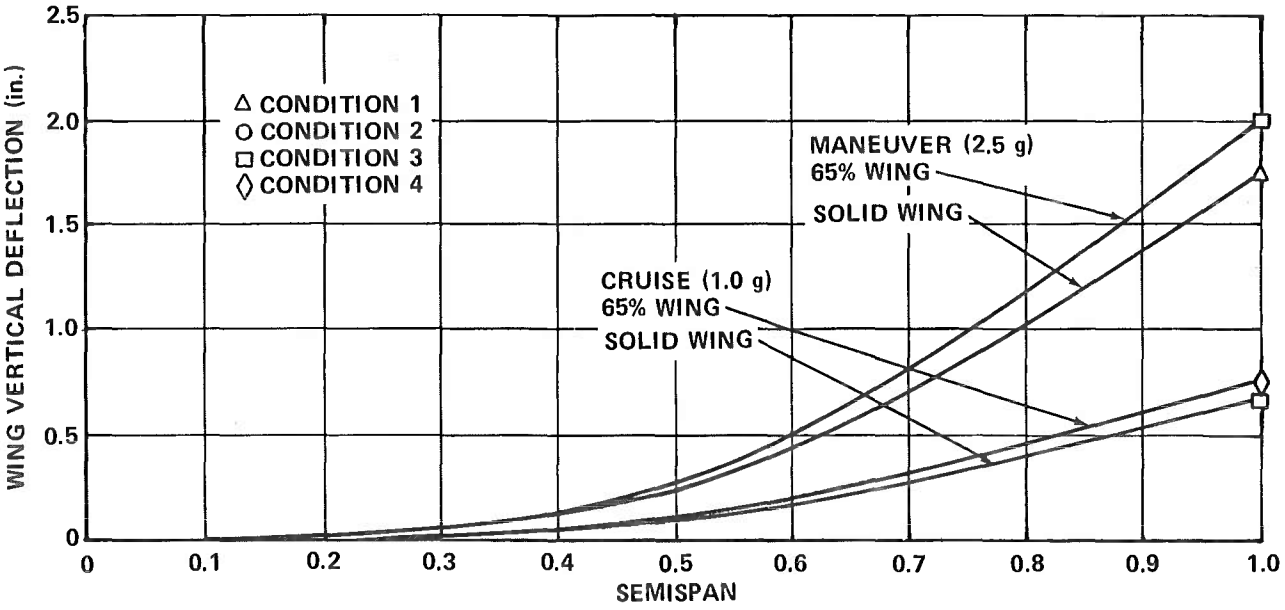

Figure 3 ATT – EFFECT ON DEFLECTION DUE TO REMOVING AFT 35% CHORD

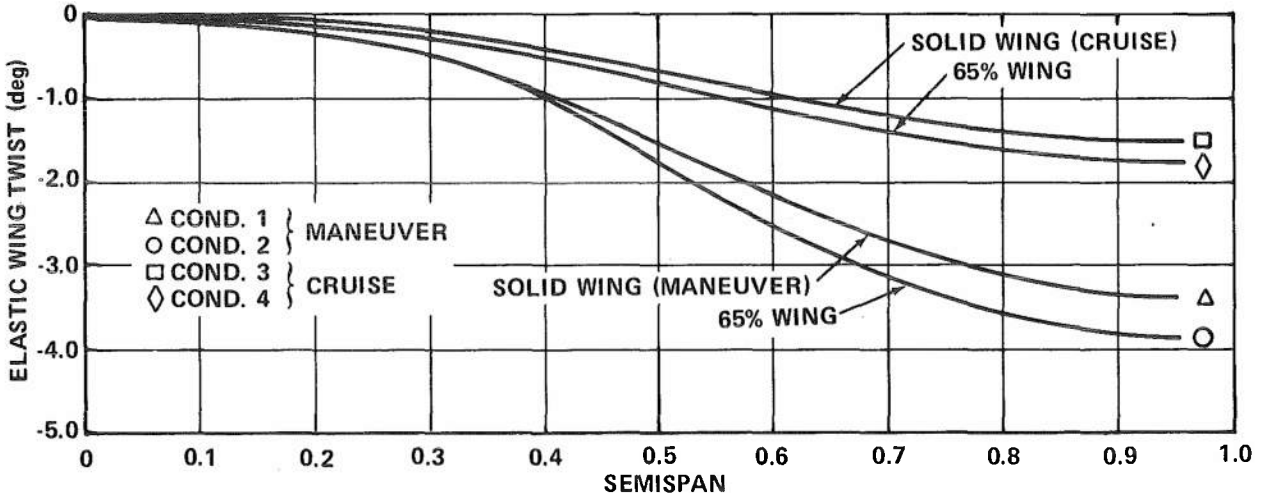

Figure 4 ATT – ELASTIC WING TWISTS

at each probe. The subsequent analyses were all directed toward demonstrating the feasibility of achieving this overall level of tolerance in deflection measurement. Note that for a 0.1 degree tolerance, the equivalent random error in deflection is approximately 3.5×10^{-3} inch.

2.4.3 Selection of Gage Location

The sole criterion used in the selection of the placement sites for strain gages on the beam was that of minimizing the levels of spurious electrical output signals resulting from applied acceleration forces. These acceleration forces might be generated by model vibrations excited by the tunnel starting process and sector-drive irregularities in the model pitching system.

The desired location of the gages is at that position on each beam segment where the bending moments arising from accelerations are equal to zero. Calculations to establish the location of these "null" points were made by writing the general bending moment equation for each segment in terms of the parameter "m" (see definition in Figure 2) for the case of a uniformly distributed load. Numerical coefficients for these quadratic equations were determined by the Cross method of moment distribution.[3] Letting the moment be equal to zero, the two "m" roots of the equation were found with the root having the lower numerical value being the one of interest.* Values for "m" were found to be: $m_1 = 0.216$, $m_2 = 0.210$, $m_3 = 0.212$. Because of the numerical similarity of these three numbers, a mean value of 0.213 for "m" is used in all subsequent applications.

It is of practical significance to determine how critical is the placement of the strain gages relative to the position $m = 0.213$ in terms of errors in measured deflections due to acceleration loads. This analysis was made by differentiating the preceding moment equations to obtain a relation defining ΔM in terms of Δm. Making use of Equation 3, calculations were made to determine the differences in y_1, y_2, y_3 when the bending moments M_1, M_2, and M_3 were modified by ΔM values corresponding to different assumed values for Δm. Values of M_1, M_2, M_3 were used corresponding to the maximum beam deflections as defined in Section 2.4.2. In order to obtain numerical values, it was necessary to specify beam cross section dimensions and beam material. The beam was assumed to be steel with a modulus of elasticity of 30×10^6 psi and with two different cross sections: 0.125 inches x 0.125 inches and 0.150 inches x 0.150 inches. A summary of the results is graphically illustrated in Figure 5 for the case of the beam with the larger cross section. The data shown are for a one "g" acceleration load and indicate a linear variation in deflection error with small displacements in gage position relative to the "null" location. It is seen that even with a gross gage displacement of 1/4 inch, the maximum deflection error (in y_3) is less than 10^{-3} inches.

*This root defines the beam position with the larger moment for any given beam deflection.

[3] Niles, A.S., and Newell, J.S., Airplane Structures, 3rd ed. (John Wiley and Sons, Inc.: New York), 1949.

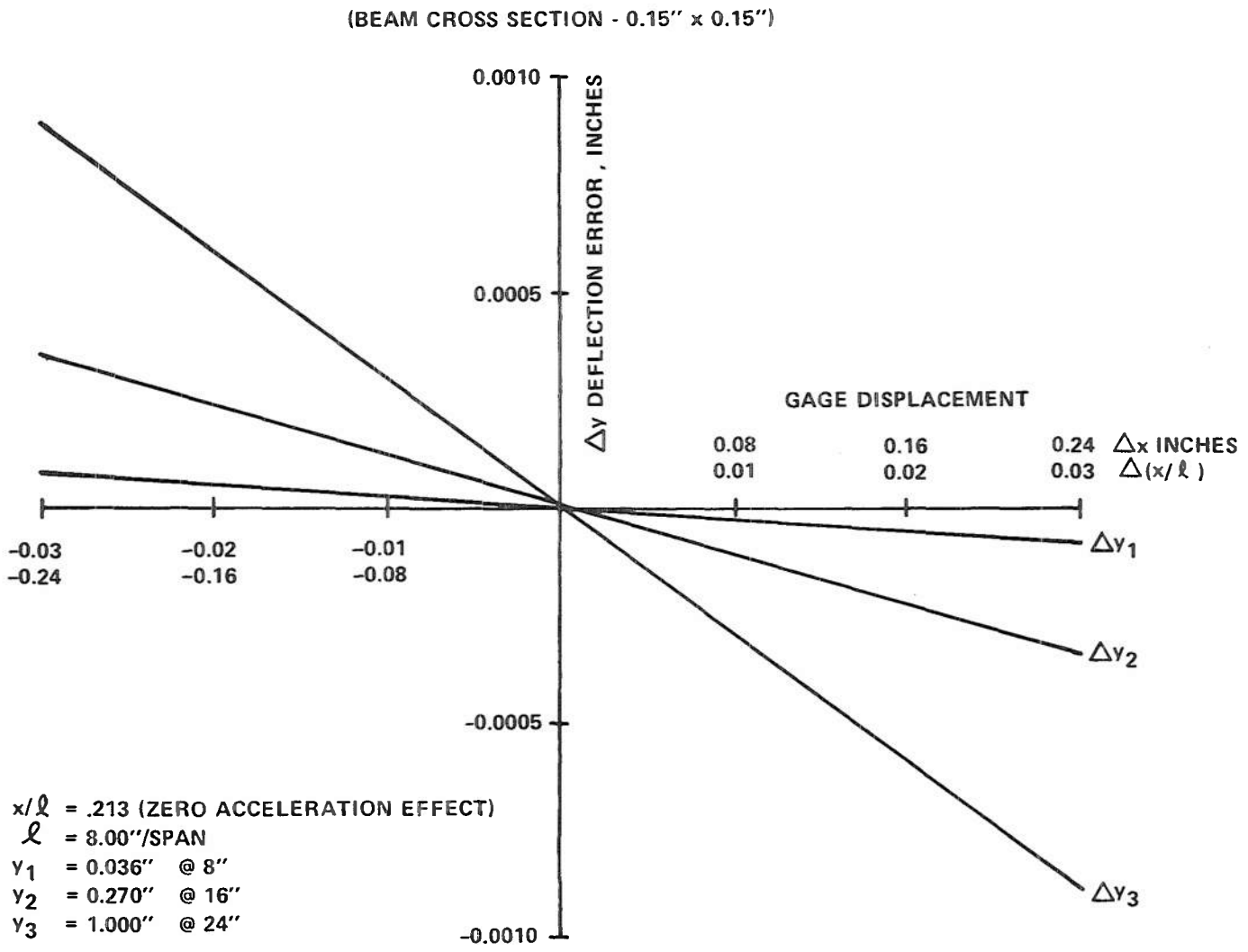

Figure 5 MEASUREMENT ERROR IN WING DEFLECTION (PER "G" ACCELERATION) FOR EACH OF THREE STRAIN GAGE BRIDGES AS A FUNCTION OF BRIDGE DISPLACEMENT FROM POSITION FOR ZERO ACCELERATION EFFECT

A parallel analysis of the two beams of differing cross sections was not continued beyond this stage since a decision was made in favor of using the larger cross section unit for the following advantages which would be realized: (1) decreased acceleration-induced errors in deflection measurement, (2) a 20% increase in bending moment per given beam deflection (resulting in larger electrical output signals) and (3) a greater choice in selection of usable strain gages associated with the increased width of the beam. The ability to use gages with larger active-grid areas permits use of larger excitation voltages and hence larger electrical output per unit strain.

2.5 ELECTRICAL CONSIDERATIONS

2.5.1 Bridge Output Levels

With the selection of the sites on the beam at which the gages are to be mounted and the firming of beam cross section dimensions, it was feasible to establish the anticipated output signal levels from the strain gage bridges. The purpose, ultimately, was to ascertain the adequacy of the signal-to-noise ratio in the light of the need to realize an accuracy of 1.5×10^{-3} inches in deflection measurement.

In a four-active-arm bridge configuration, two of the gages are mounted on the upper surface of the beam and two on the lower.* From stability considerations, the amount of energy dissipated per unit area of the gage is limited and specified according to the thermal sink characteristics of the substrate to which the gage is bonded.(4) Since the signal output level varies directly with the input voltage, it is advantageous to maximize strain gage area. The use of gages with higher nominal resistances also is a factor in obtaining increased output levels. Various other methods are available to increase output; e.g. a change in beam design to increase strain per unit deflection, use of an eight-active-arm bridge, etc.

With these considerations in mind, the choice was made of a metal foil strain gage, made by Micro-Measurements, and designated as type SA-06-125AC-350. Basically, this designation signifies that it is a fully-encapsulated, Constantan gage compensated for use on a substrate with a coefficient of linear expansion of 6 PPM/°F. It has a grid width and length equal to 0.125 inch and a resistance of 350 ohms. These grid dimensions require that the gages be mounted on the beam in a series (back-to-back) rather than a parallel (side-by-side), arrangement.

Using a recommended power density level of 1.5 watts per $in.^2$, a gage factor of 2.05 and maximum strain levels as determined from Equation 4, the anticipated electrical signal levels were calculated. The results are

*Assuming deflection takes place in a vertical plane.

(4) "Strain Gage Excitation Levels," Tech Note TH-127, Micro-Measurements, Romulus, Michigan, August 1968.

summarized in Table 1 which also lists the magnitudes of the reaction loads, bending moments and strains. Based on experience at Calspan, these signal levels were judged to be reasonable pending a more detailed evaluation relative to the estimated system noise levels (See Sections 2.5.2 and 2.6.2).

Table 1
STRAIN GAGE BRIDGE MAXIMUM
SIGNAL LEVELS – COMPUTED FOR 0.15 · INCH SQUARE BEAM

DEFLECTION, y* (INCHES)	SEMISPAN POSITION	REACTION (LBS)	BENDING MOMENT (INCH-LBS)	STRAIN (MICROSTRAIN)	SIGNAL OUTPUT (mV)
0.036	0.25	1.40	1.31	77.4	0.9
0.270	0.50	-3.28	4.63	274	3.2
1.000	0.75	1.77	11.15	660	7.7

* 2.5 g CONDITION, 65% WING

STRAIN GAGE DATA: METAL FOIL TYPE, GRID SIZE $^1/_8$"L x $^1/_8$"W, 350 OHMS
BRIDGE VOLTAGE: 5.7 VOLTS (POWER DENSITY = 1.5 WATTS/SQUARE INCH)

2.5.2 Signal Conditioning Equipment

Use of strain gage sensors requires provision to be made for a source of power input into the gages as well as a means for amplifying the low level signals that these units provide. Gages operate equally well on either a-c or d-c excitation. If the former is used where dynamic measurements are involved, an adequate ratio of carrier frequency to modulation frequency must be assured.

Operation on d-c excitation will necessitate the use of a battery as a power source since even the best of the a-c operated power sources of d-c voltage possess ripple and noise levels of the order of 40 microvolts rms (100 microvolts peak-to-peak). In comparison with the signal levels shown in Table 1 and the 1.5×10^{-3} inch objective in deflection accuracy, this noise level is unacceptably high. For purposes of operational flexibility and freedom from potential ground loop problems, a complete and separate electrical system should be employed with each bridge. The practice of using a power supply and amplifier unique to each bridge circuit is commonly observed in wind tunnel gaging systems.

A typical strain gage system is schematically illustrated in Figure 6. For maximum accuracy a six-wire arrangement is used. R_g represents the strain gage resistance while r_t and r_o represent bridge balance compensating resistances (against thermal effects) in a shunt-type arrangement. Resistance r_s is used in a series-type compensation arrangement to render the bridge sensitivity to deflection independent of temperature. A means for calibrating the circuit is provided by R_c, a precision resistor, placed in shunt with one

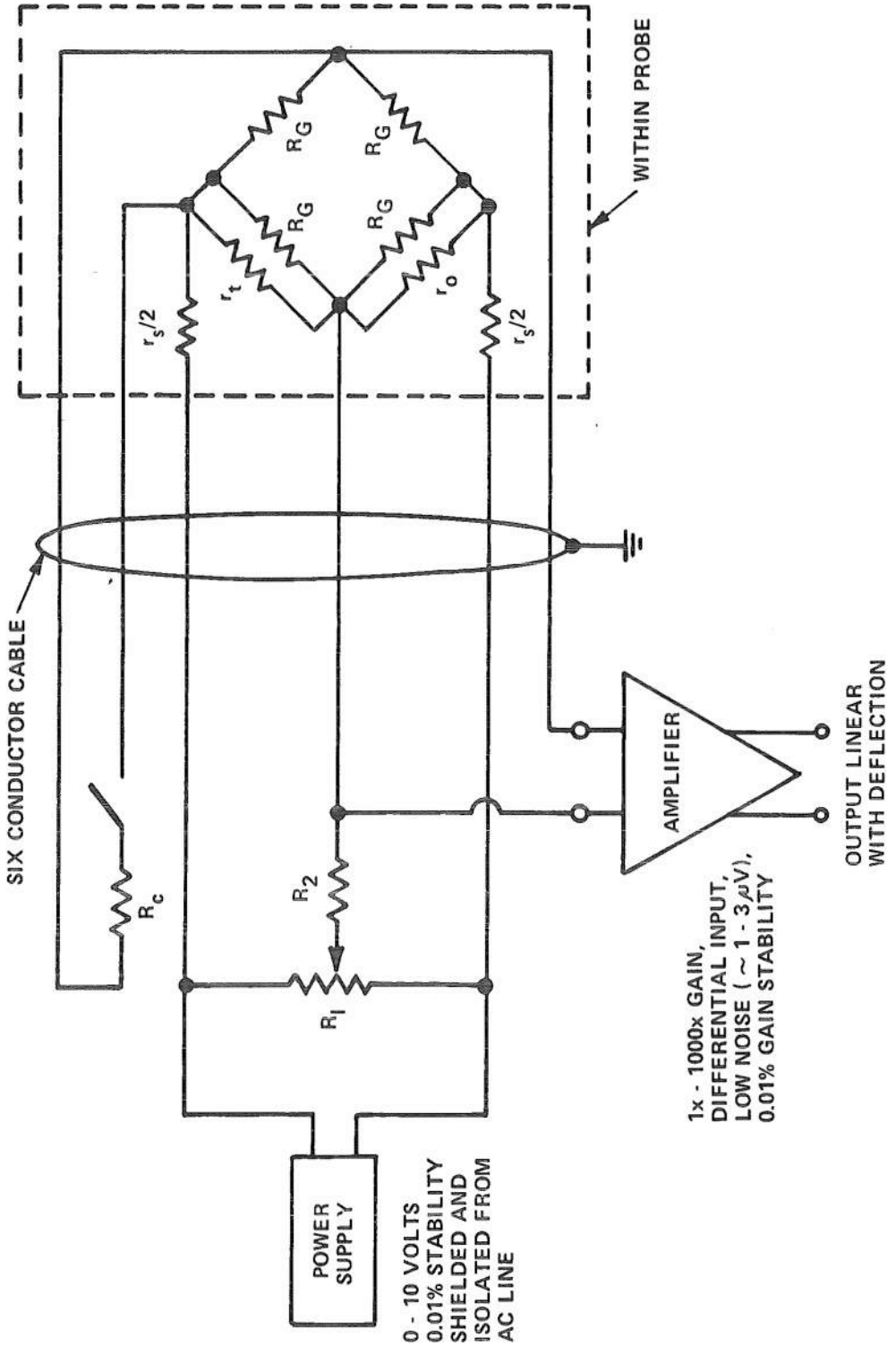

Figure 6 SCHEMATIC - TYPICAL STRAIN GAGE BRIDGE CHANNEL (3 PER PROBE)

of the arms of the bridge. Manual balancing of the electrical output of the circuit is accomplished by the potentiometer R_1.

Input noise levels of amplifiers are directly related to the bandwidth capabilities; wide bandwidths are synonymous with high noise levels. Consequently, it is necessary to define the minimum bandwidth required to meet the requirements of the HIRT application. Preliminary information supplied by AEDC on the starting loads of the tunnel indicated they would be so gradual that model and sting vibrations would not be excited (later data, see Section 2.6, introduced the need to accommodate model vibrations). Thus the principal requirement for bandwidth definition was that of following wing deflection changes with pitch angle. The following assumptions were made to simplify the computations: (1) the high frequency roll-off characteristic of the amplifier could by approximated by that of a simple RC low pass filter (a very reasonable assumption), and (2) the wing deflection varied linearly with pitch angle. Using a ramp-type input function, it was computed that a maximum steady-state lag equivalent to a deflection 1×10^{-3} inch would exist for a wing deflecting from 0 to 1 inch in 3 seconds using an amplifier with a corner frequency of 53 Hertz. Commercial amplifiers of suitable gain and bandwidth are available with very low noise levels. For example, one unit* with a bandwidth from dc to 100 Hz and a gain of 1000X has an input noise level of ± 1.5 microvolts. Using the method of Appendix B, it can be shown that the maximum error in beam deflection due to this uncertainty in signal level is $\pm 0.3 \times 10^{-3}$ inch and occurs at η_3 . This error is acceptably small relative to the $\pm 3 \times 10^{-3}$ inch tolerance corresponding to ± 0.1 degree accuracy objective in wing twist measurement.

2.6 DYNAMIC RESPONSE

2.6.1 Mechanical Aspects

Subsequent to the completion of the Phase I effort, an internal document from AEDC was received which dealt with detailed performance requirements of the HIRT model deformation measuring system.(5) The problem considered in this document may be stated in the following simplified form. Model wing natural frequencies are estimated as approximately 50 Hz and characterized by a very low damping coefficient. This wing natural frequency may be excited by such external forcing functions as tunnel start-up loads as well as sting sector drive imperfections. Reference 5 concludes, as stated earlier in

*Hewlett-Parkard Differential Amplifier, Model 8875A.

(5) Starr, R.G., "A General Definition of Model Deformation Measurement System Requirements" AEDC Memorandum, March 1, 1974.

Section 2.5.2, that the starting process will be sufficiently gradual that any model oscillations that are excited will decay to negligible amplitude by the time steady state flow is achieved and data collection is initiated. Of more concern are the intangible, extraneous inputs, such as imperfections in the sector drive, which are likely to be present to excite the model during the data-collection portion of the test. Recognizing that these sources, and the magnitude of their effect, cannot be systematically analyzed, Reference 6 concludes that "...a deformation measurement system which is capable of following relatively small amplitude oscillations at 50 Hz or less is clearly advantageous." Thus this section considers the consequences of a 50 Hz forcing function in terms of the mechanical response of the strain-gage beam.

The natural frequency, f_n, of a uniform beam in bending is given by the following general formula.

$$f_n = \frac{a_n}{2\pi}\left(\frac{EI}{\mu l^4}\right)^{1/2} \tag{7}$$

where a_n = a coefficient dependent on the type of beam support and the vibrational mode

μ = mass per unit length

l = beam length

For a solid steel beam of square cross section, the preceding equation may be recast in the following form.

$$f_n = 9.3 \times 10^3 \frac{a_n h}{l^2} \tag{8}$$

Where h is the thickness of the beam.

Reference 5 concludes that the maximum half-amplitude of the wing vibration due to tunnel starting loads will be approximately 1% of the static deflection. While it is doubtful that extraneous excitation loads will equal the tunnel starting load in magnitude, nevertheless this amplitude criterion is assumed to apply for the sake of a conservative analysis. Thus a peak amplitude of ±0.01 inch would be expected at the furthest outboard reaction point of the strain gage beam (3/4 semi-span) where the maximum static deflection is one inch. To simplify the analysis, consider that the entire 8-inch length of the outboard section of the beam experiences a uniform acceleration corresponding in magnitude to a forcing function of 50 Hz with a 0.01-inch half-amplitude. This segment of the beam may be considered equivalent to a simply-supported beam for which a_n (Eq. 8) is equal in magnitude to π^2 for the fundamental mode of vibration. Substituting numerical values for the beam dimensions, the natural frequency is calculated to be 215 Hz. For a system with very low damping characteristics, the output-input amplitude ratio is given by the following expression

$$\left[\frac{1}{1-(f/f_n)^2}\right]$$

where f is the forcing function frequency applied to a system of natural frequency f_n. Thus, the vibration amplitude of the beam segment would be increased by approximately 6% at a frequency of 50 Hz relative to the amplitude of the forcing function (0.01 inch). Thus, no serious resonance phenomena are encountered and, for analytical purposes, this amount of augmentation is of negligible import.

The peak acceleration load imposed by the wing vibration at 50 Hz and a peak amplitude of 0.01 inch is approximately ±2.5 g. Based on the sensitivity of measurement error in wing deflection due to acceleration, as shown in Figure 5, a deflection error of $\pm 0.2 \times 10^{-3}$ inch would be incurred assuming a ±0.02 inch misalignment of the strain gages from the "null" position on the beam.

In reality, the beam will not experience a uniform acceleration along its length, rather, the acceleration will be proportional to the local amplitude of wing deflection. Since the simple analysis has demonstrated the very small levels of vibration effects, the complexity of the more rigorous analysis was not considered a worthy expenditure of effort.

2.6.2 Electrical Consequences

Previous requirements on the frequency response of the strain gage electronic system were evaluated in Section 2.5.2 wherein it was determined that a bandwidth of 0-50 Hz would be adequate to cope with the model pitch rate. Such a bandwidth would be grossly inadequate to accurately process a 50 Hz signal. The consequences would be (1) a reduction of peak amplitude by 29.3% and a phase lag of 45 degrees (or a time lag of 2.5×10^{-3} second).

Analysis was made of the bandwidth requirements to faithfully follow a 50 Hz signal frequency. To provide a conservative margin of safety, the anticipated half-amplitude of the oscillation was increased by a factor of two (relative to that used in Section 2.6.1 to ±0.02 inch.

Procedural details of the analysis which lead to an amplifier bandwidth requirement of 0-1000 Hz are given in Appendix C. An amplifier with this bandwidth will produce a maximum error (due to phase lag) of one thousandth of an inch in the measurement of the instantaneous deflection of a model wing oscillating at 50 Hz and a half-amplitude of 0.02 inch. Fidelity of the peak amplitude is better than 0.1%.

An increased bandwidth requires the tolerance of a larger input noise level in the amplifier. Typical noise levels for high-quality instrumentation amplifiers at a gain of 1000X and a bandwdith of 0-1 kHz with an input impedance of ~ 1k ohms are ±3 microvolts. This is exactly twice the noise level used in the analysis of Section 2.5.2 wherein the maximum deflection

error on a root-sum-square combination of the contributory inputs (see Appendix B) was determined as 3×10^{-4} inch. Using these same computational methods, the maximum root-sum-square deflection error was determined as 6×10^{-4} inch. This value is still well within acceptable limits despite being based on very conservative estimates.

2.7 ERROR ANALYSIS

In an overall error analysis of an instrumentation system, it is common practice to include only those sources of error that are random in nature or are otherwise indeterminate. Electrical noise is an example of the former while signals attributable to acceleration forces (whose levels are not known) are examples of the latter. Such system "errors" as may be ascribed to nonlinearities, temperature effects, pressure effects, system input-output time lags, probe misalignment in installation (in roll angle), etc. are not properly included in a system error analysis since they are reproducible and predictable. Consequently, corrections may be made based on calibration data.

By way of a summary, some comments on the correctable items are appropriate. Thermal compensation of the strain gage circuits is feasible. Perfect compensation over a sizable range of temperatures is rarely possible so that a compromise must be made. The residual temperature sensitivity will be small and consequently not a strong function of temperature. Thus, the use of second order corrections is practical even without a precise measure of gage temperature. Pressure effects on strain gages have been shown to be small. With a four active arm bridge, self-compensation will occur to the extent that the pressure sensitivity of the individual gages is sensibly the same. Glue line quality (freedom from voids) will be a critical factor. In any event, these effects should be small, and if necessary, correctable with even an approximate knowledge of ambient pressure levels.

For reasons cited in Section 2.6.2, it is essential in critical applications to minimize the bandwidth of the electronic system to maximize the signal-to-noise ratio. A bandwidth of 1 kHz has been shown to reduce maximum deflection errors to 1×10^{-3} inch in measurement of a wing oscillating at 50 Hz due to phase lag. While a wider bandwidth would reduce such phase lag error further, increased noise would result. Also, lag error is predictable and hence correctable.

Error can also be incurred if the sensitive axis of the beam is not properly aligned (upon installation in the model) at a right angle to the wing chord. If the wing-probe combination is calibrated as a unit, then any misalignment is corrected for in the calibration results. Since the error is a cosine function of the misalignment angle (in roll about the probe axis), it can be verified that a 0.1 degree tolerance in angular alignment will result in negligible error for the case where a precalibrated probe is installed in a wing. Since such installation tolerance is feasible, errors from roll misalignment may be treated as negligibly small.

Sources of random error, as defined above, are of mechanical and electrical origin.

Mechanical

- bearing radial play
- bearing O.D./bore diameter play
- gage placement (error/g)

Electrical

- amplifier input noise
- non-common mode noise
- amplifier gain stability (short-term)
- power supply stability (short-term)

Bearing play will contribute directly to deflection error whenever the sign of the reaction load changes at the beam. While mechanical pre-load may be utilized to preclude such a change of polarity in the reaction load, the physical complexity engendered by such techniques within the small confines of the bore does not appear to be necessary or desirable. By selecting bearings, radial play equal to $\pm 1 \times 10^{-4}$ inch is considered realistically feasible. Play between the outside diameter of the bearing assembly* and the inner diameter of the bore into which the probe will be inserted has been estimated as less than 5×10^{-4} inch using available fabrication technology. For analytical purposes, a value of 3×10^{-4} inch will be assumed.

Strain gages will be installed at beam locations calculated to produce minimal response to acceleration loads. A conservative (generous) estimate would assume placement within ±0.02 inch of the desired "null" location. As shown in Section 2.6.1, the maximum error in deflection due to this gage placement tolerance and expected peak acceleration loads is 0.2×10^{-4} inch and occurs at the outboard, y_3 , position on the beam.

Deflection measurement errors attributable to amplifier noise were computed in Section 2.6.2. For a system using three amplifiers (one per each bridge), the maximum magnitude of this error was found to be 6×10^{-4} inch. Power supply and amplifier gain stabilities both directly affect the system electrical output signals. Stabilities of ±0.01% are realizable for both of these units. Using the methodology of Appendix B, these stability tolerances translate into maximum deflection errors of 6×10^{-5} inch based on a root-sum-square summation.

There is a type of circuit noise, which for a lack of standard terminology, may be referred to as non-common-mode noise. Using a differential-

*The bearing will be fitted with an annular ring.

input amplifier, a noise signal (common mode) appearing simultaneously at each of the two amplifier terminals will automatically cancel. Common-mode noise includes such types as hum pick-up, for example. Electrical noise generated in interconnecting cables as the result of mechanical vibrations is one example of non-common-mode noise. An estimate of this type noise can only be a conjecture based on experience. An estimate of a noise level equivalent to ±0.5 microstrain is probably realistic. Assuming this equivalent noise level for each of the three circuits, the maximum root-sum-square error in deflection is 1.2×10^{-3} inch and is the largest identifiable source of error.

A summary of the random errors is given in Table 2. A simple sum of the individual errors is not a reasonable way to combine them since the probability of all random errors simultaneously being of the same sign and at maximum amplitude is extremely remote. Such a sum does correspond to an extreme possible value. The root-sum-square method of combining errors is a more reasonable approach that is in common practice. As shown in Table 2, the maximum error is estimated to be 2.52×10^{-3} inch and the root-sum-square value is 1.40×10^{-3} inch. These values may be compared with the somewhat arbitrary objective of 1.5×10^{-3} inch in deflection measurement which corresponds to a wing twist angle of 0.04 degrees. Thus the random errors which have been identified satisfy this criterion on the root-sum-square basis. Even the maximum estimated error is equivalent to a twist angle error of less than 0.1° (or a deflection error of 3×10^{-3} inch).

Table 2

SUMMARY OF RANDOM SOURCES OF ERROR AND THEIR MAGNITUDES

SOURCES	DEFLECTION ERROR (thousandths of an inch)
MECHANICAL	
BEARING RADIAL PLAY	± 0.1
BEARING/BORE PLAY	± 0.3
GAGE PLACEMENT	± 0.2
ELECTRICAL	
AMPLIFIER NOISE	± 0.6
AMPLIFIER GAIN STABILITY	± 0.06
POWER SUPPLY STABILITY	± 0.06
CIRCUIT NOISE	± 1.2
SIMPLE SUM OF ERRORS	± 2.52
ROOT-SUM-SQUARE ERROR	± 1.40

The Phase I analytical study thus indicated that the model deformation measurement goals set for the HIRT application appeared to be feasible of attainment with a dual-probe arrangement using strain-gage sensing techniques.

2.8 EVALUATION OF MODEL POSITION INDICATOR SYSTEMS

The measurement of model pitch angle was assigned a low priority with rather limited effort devoted to an assessment of the applicability of existing instrumentation for on-board type sensing. Accuracy objective was ±0.1 degree with an available (in model) spatial volume defined by a cavity 6 inches in diameter and 11 inches in length.

A review of current wind tunnel practice failed to identify any system which would meet both the static and dynamic requirements of the HIRT application. Rather, consideration was given to such likely devices as displacement gyroscopes, rate gyroscopes (with an external integrator), linear accelerometers and a package comprising a rate gyroscope and a linear accelerometer.

A displacement gyro possesses the capability of providing information on both the static and dynamic values of pitch angle directly. The large size of these devices would appear to present serious model installation problems considering the need for a sealed container for pressure protection. In addition, the overall accuracy is estimated as no better than one-half degree.

The rate gyro is attractive from the standpoint of small size and reliability. While capable of meeting the accuracy goals (with suitable integrating circuitry), this device will not provide a measure of the initial pitch angle of the model.

A linear accelerometer is useful for accurate sensing of static position information; however, model vibrations might be expected to compromise the dynamic accuracy. It was concluded that the most satisfactory system would be one consisting of a linear accelerometer (for static position data) and a rate gyro (for dynamic data). Both units would be envisioned as enclosed in separate pressure-tight containers and equipped with electrical heaters. Such a combination would constitute a complete model position indicator. Since the initial model position may be measured very accurately (prior to a test run) with a manual device such as an inclinometer, this option may be exercised in lieu of the accelerometer.

Appendix D contains further details on component sizes, weights, costs, sources, and operating life as well as system block diagrams.

2.9 MODEL ADAPTATION

The strain-gage probe is an entirely self-contained sensor which provides an electrical output directly related to probe deflection. Two probes will be used within a model wing by being fitted into long holes provided for this purpose. Probes may assume one of two possible configurations. Configuration A is envisioned as comprising a strain-gage beam installed within a precision tube or encasement. Configuration B would consist simply of the strain gage beam itself (including the roller-bearing reaction points).

In the first configuration (A), the beam is precisely fitted into a thin-wall encasement which then must be fitted to the hole in the model wing. This arrangement has several serious drawbacks. To preserve its dimensional integrity, the encasement must have a sizable wall thickness. With the wing bore diameter limited to about 0.3 inch to maintain a reasonable chordwise separation between probes and to accommodate probe lengths up to 3/4 semi-span, the beam dimensions would need to be constrained to very small diameters allowable within the encasement. Mechanical complexities are introduced. In addition, precision tolerances are required on the following: inside and outside diameters of the encasement and the bore diameter in the wing.* The second method only requires that a hole is precision machined in the wing and the bearing collars are fitted to this bore diameter. Absence of an encasement tube also permits the beam to assume larger proportions because of the ability to use a larger bore diameter. Besides being simpler and less expensive, this latter configuration offers the better potential accuracy because of the fewer critical requirements in matching dimensions of components. Experience during Phase II of this program has shown that small bore diameters up to 2 1/2 feet in length can be held to tolerances of tenths of thousandths of an inch.

The necessity for boring holes in the model makes it desirable that the model have a two-piece wing so that the wing root is accessible for drilling operations. For models with a one-piece wing, consideration should be given to the feasibility of drilling inward from the wing tip. It is also desirable to bore the wing holes in raw stock before the wing airfoil shape is machined because it is a critical operation in which excessive run-out could result in a useless wing. The bore drilled in the encasement used in the Phase II tests experienced a run-out of 0.15 inch over a length of 3 feet. This is much larger than the one-thousandth inch per inch run-out the vendor expected to adhere to and should not be taken as representative of present technology.

Conflict with other instrumentation in the wing, such as pressure orifices and channels for routing pressure tubing, is probably unavoidable for a two-probe system. Because of the diversity of models which might be tested and other instrumentation requirements, it is not possible to draw universally applicable conclusions. It is probable that at least one wing of a model may need to be solely devoted to wing deflection measurements. For reasons of accuracy, it is necessary to maintain a minimum separation between probes of the order of three inches as measured along a chord. Requirements such as these mitigate against the possibility of fitting two probes in among other instrumentation competing for space.

The strain-gage probe senses deflection with respect to its fixed end which is visualized as being attached to the model at the wing root. An error in the measurement of wing deflection will thus be incurred to the extent that a deflection in the wing root occurs relative to a reference

---

*It is possible to provide an oversize hole in the wing and fill it with a material of low melting temperature to hold the probe rigidly in place.

plane in the fuselage. Again, this is a problem that will need to be resolved on a model-to-model-basis. It is conceivable that suitable structures can be found, or added, in the wing root area that can be instrumented with strain-gages to measure such deflections. Corrections to probe data would then need to be made.

Calibration of the model deformation measuring system should be capable of being performed at normal ambient conditions with the data applicable to the range of HIRT operating environments. Using configuration A, the probe may be calibrated as a separate entity or after installation in the model. Configuration B would best be calibrated only after installation in the model to insure that there were no anomalies associated with the installation (binding, excessive play, etc.).

With sufficient care exercised, the strain gage sensors can be made independent of temperature insofar as input/output performance is concerned. Temperature compensation is designed to preserve bridge zero balance in the presence of temperature changes principally by correcting for apparent strain. Apparent strain results from differential expansion between the beam and the gages. Gages compensated for use on steel beams, for example, are available. Since a manual balance control is provided in the circuitry, such compensation is only required for any temperature change in the sensor occurring during a test run. During a typical 3-second test run, the beam temperature should be substantially constant despite a change in airflow temperature and model aerodynamic heating. Temperature compensation is also required to preserve the constancy of bridge sensitivity which is affected by a changing gage factor with temperature.

It is important to recognize that since the beam is simply a follower of the wing shape (and does not affect the stiffness of the wing), the change of beam elastic modulus with temperature must not be thermally compensated. The strain in the beam is simply dependent upon its deflected shape and independent of temperature.

Calibration involves the determination of the matrix coefficients for the following equation

$$\begin{bmatrix} y_1 \\ y_2 \\ y_3 \end{bmatrix} = \begin{bmatrix} \text{COEFFICIENT} \\ \\ \text{MATRIX} \end{bmatrix} \begin{bmatrix} e_1 \\ e_2 \\ e_3 \end{bmatrix} \tag{7}$$

where e_1, e_2, e_3 are the electrical outputs from the three respective strain gage circuits. The wing must be subjected to known deflections (assuming in-model calibration) in such a manner that a sufficient number of independent equations relating y and e are obtained to evaluate the nine coefficients of the matrix. From statistical considerations, the greater the number of calibration points the better the precision of the matrix coefficients. With the matrix coefficients established, the electrical signals from the probe may then be used to compute the three deflections. Section 3.5 discusses an actual calibration of a prototype probe.

Section 3.0
PHASE II - EXPERIMENTAL STUDIES

3.1 SCOPE AND OBJECTIVES

The principal objective of the Phase II studies was to provide experimental substantiation of the capability of the strain-gage-beam model deformation measuring system to attain the accuracy and the precision postulated by the analytical Phase I study. As a consequence, Phase II was concerned with detailed mechanical design, fabrication of hardware and bench check demonstrations of system characteristics.

An in-depth discussion of the scope of the experimental program took place at AEDC following the oral briefing on the Phase I study results*. There was mutual concurrence on the desirability of conducting a comprehensive test program which would include dynamic tests, deflection/torsion tests and an evaluation of temperature effects on a two-probe configuration installed in a simulated model wing. Budgetary constraints dictated that a less ambitions program would need to be implemented yet one that provided a critical evaluation of the essential aspects of the strain gage probe technique. It was therefore decided that only a single probe should be fabricated and tested.

A simple, metallic slab, called an encasement, would simulate a spanwise element of a model wing and would be bored to accept the strain gage beam. A suitable test fixture would also be fabricated which permits the conduct of the following test effort: (1) precise measurement of encasement deflections and corresponding strain gage outputs (all at ambient conditions), (2) measurement of encasement deflections and corresponding strain gage outputs in the presence of applied twist angles (all at ambient conditions) and (3) the measurement of strain gage outputs in response to the application of known displacements of the encasement at reduced temperatures. Data from part (1) would be used in the determination of the matrix coefficients in the equation expressing encasement deflections in terms of the output signals from the three strain gage bridges**. Use of these matrix coefficients would permit a correlation between measured and calculated deflections.

Part (1) tests are designed to explore repeatability and accuracy of measurement by permitting the effects of bearing "play" and system hysteresis to be exercised. Parts (2) and (3) are structured to identify the magnitudes of the errors involved in determining encasement deflections from strain gage signals as the result of encasement twist angle and ambient temperature variation respectively.

---

*23 January 1974

**See Equation 7

3.2 DESIGN AND FABRICATION

3.2.1 Strain Gage Probe and Encasement

Design of the strain gage beam generally followed the tentative geometry and dimensions characterized in Section 2.0. The basic beam cross section measures 0.15 inch x 0.15 inch except for the areas adjacent to the three reaction points. These enlarged sections, which accommodate the ball-bearing assemblies, have been designed to maintain a constant (approximately) section modulus along the beam length to impart the characteristics of a uniform cross section beam. Figure 7 is an engineering drawing wherein the beam is identified as item -6. The beam was fabricated from 0.75-inch diameter stock of a precipitation-hardened, high-strength steel (VASCOMAX 300 CVM) which is representative of the type of metals that will be used in the fabrication of HIRT wind tunnel models.* To economize on machining time, the beam thickness is constant throughout its length and only the width is varied to accommodate the bearing assemblies at the reaction points. Note also that scribed lines are provided on the beam at 1.70 inches** from the fixed end and the two reaction-point centers to locate the strain-gage installations. The fixed end of the beam is provided with a pilot shoulder to accurately center the beam within the bore of the encasement. Clearance holes are also drilled through the base to bring out the electrical leads from the strain gage bridges. Mounting holes, as well as dowel pins for preserving very accurate rotational orientation between the beam and the encasement, are provided in the circular base.

Details of the bearing assembly are shown in Figure 7 as item -9. Bearings selected were type SRO New Hampshire Miniature Ball Bearings with an outer diameter of 0.1562 inch and an inner (shaft) diameter of 0.0468 inch. These bearings have a radial-play tolerance within 2×10^{-4} inch. Since bearing frictional torque decreases with bearing diameter, the smallest bearings were selected consistent with long life expectancy under the applied loads.

Each bearing was fitted with a wheel assembly (item -12) whose diameter was precisely fitted to the bore diameter of the encasement. Note that the radius of the wheel periphery (in a plane containing the bearing shaft axis) is smaller than the bore diameter so that a single-point contact occurs between the bore and the wheel at its maximum diameter.

The probe encasement, shown as item -5 in Figure 7, provides both a housing for the strain-gage beam and serves the function of a spanwise element of a model wing. Fabricated from 1.5-inch diameter stock of VASCOMAX 300, the encasement contains a relatively long (25.25 inch) bore of small diameter (finished diameter was 0.3124 inch +0.0001 inch). This bore was produced by the use of precision gun-drilling and honing techniques*** to produce a bore

---

* See Reference 2.

** (x/ℓ = 0.213, ℓ = 8.00 inches)

*** The bore was machined by the 20th Century Machine Company, Sterling Heights, Michigan.

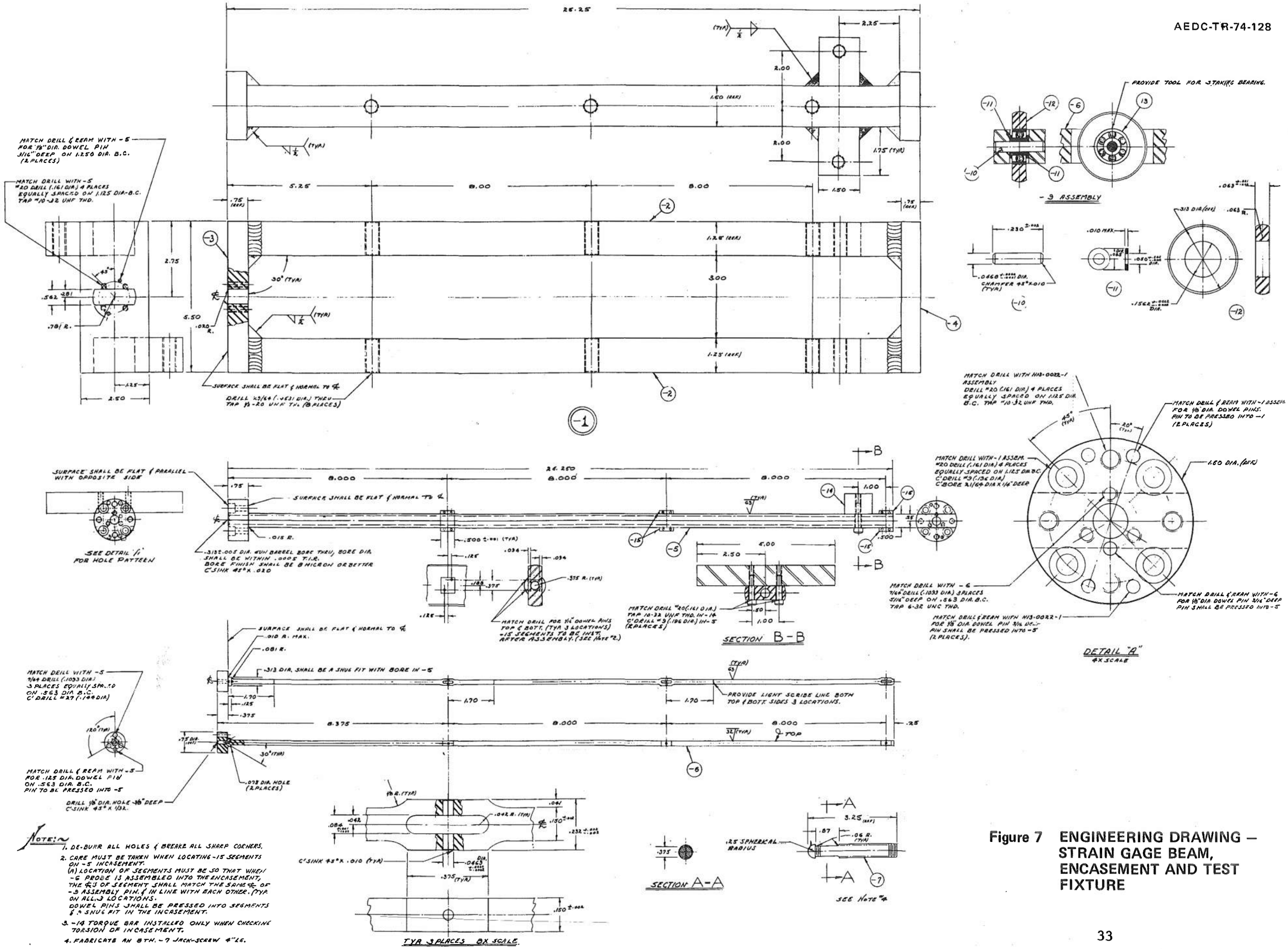

NOTE:

1. DE-BURR ALL HOLES & BREAKE ALL SHARP CORNERS.
2. CARE MUST BE TAKEN WHEN LOCATING -15 SEGMENTS ON -5 INCASEMENT:
   (a) LOCATION OF SEGMENTS MUST BE SO THAT WHEN -6 PROBE IS ASSEMBLED INTO THE ENCASEMENT, THE ℄'S OF SEGMENT SHALL MATCH THE SAME ℄ OF -3 ASSEMBLY PIN ℄ IN LINE WITH EACH OTHER. (TYP. ON ALL 3 LOCATIONS.
   DOWEL PINS SHALL BE PRESSED INTO SEGMENTS & A SNUG FIT IN THE INCASEMENT.
3. -14 TORQUE BAR INSTALLED ONLY WHEN CHECKING TORSION OF INCASEMENT.
4. FABRICATE AN 8TH. -7 JACK-SCREW 4" LG.

Figure 7 ENGINEERING DRAWING — STRAIN GAGE BEAM, ENCASEMENT AND TEST FIXTURE

of uniform diameter and a high quality surface finish*. These requirements are made tractable by relaxing specifications on the exact numerical value of the bore diameter and bore straightness. For example, the bore diameter was specified to be 0.313 inch ±0.005 inch and was eventually finished to 0.3124 inch ±0.0001 inches. Runout was approximately four thousandths of an inch per inch of bore length and thus much larger than the one thousandth of an inch per inch the vendor anticipated holding. This runout was not bothersome since the subsequent machining operations were made with respect to the bore itself. While this runout experience may be atypical (unusally large) it does imply that it is preferable to ultimately machine the model wing to the bore(s) rather than bore a finished wing since excessive runout may result in a ruined wing. Run-out or curvature of the bore is inconsequential from the standpoint of the strain gage beam.

Cross-sectional area of the encasement is designed to achieve mechanical integrity in the transmittal of deflections to the internal beam and yet have sufficient compliance so that the forces required to deflect it are reasonably small. The latter feature places lesser rigidity requirements on the test jig used to apply these loads. The encasement has two plane-parallel surfaces which are machined parallel to the internal bore and provide an encasement thickness of 0.50 inch.

A precision counterbore is machined into the bore at the base of the encasement to accept the pilot shoulder on the beam. Also holes are match-drilled in the encasement base and the beam base for dowel pins to assure that the upper and lower plane surfaces of both units are parallel upon assembly. The base also provides holes for screws to attach the beam to the encasement and the encasement to the test fixture.

Three sets of cylindrical segments (item -15, Figure 7) were installed on the encasement to aid in the optical measurement of beam deflection. One segment was installed on the upper surface and one on the lower surface of the encasement at each of the three reaction points. These segments were centered with respect to the center of the bearing shaft. To provide accurate deflection measurements with the beam subjected to torsion, the radius of curvature of the segment coincides with the center of the bore.

A torsion bar (item -14) bolts unto the encasement near its free end and, by means of differential screws set into the test fixture, torsion can be applied to the encasement. Figure 11 clearly shows the entire test unit assembly.

3.2.2 Test Fixture

Evaluation of the strain-gage probe concept involves the demonstration of the consistency of the relationship between the electrical outputs and the mechanical inputs (deflections) to the stipulated tolerances over the range of variables associated with the HIRT operations. To achieve this end, a test fixture was designed and built which was capable of loading the

*Less than 8 microinch.

encasement and facilitating an accurate, precise measurement of the deflections imposed. It was of a size consistent with the spatial capability of an available environmental chamber. Design considerations were principally motivated by the need to achieve economy in both design and fabrication costs. The geometrical details of the fixture are given in the upper portion of Figure 7.

Basically, the fixture has an elongated "D" shape with the long dimension horizontally oriented. The component members are ground steel-plate pieces which are welded together for adequate rigidity. The encasement attaches to one end of the fixture which is slotted to permit the encasement to project internally into the enclosed space of the fixture. Holes are drilled and tapped in both the upper and lower arms of the fixture to receive loading screws for deflecting the encasement. These six screws are completely independent of one another and can impose both positive and negative deflections. Also attached at one end of the test fixture are two outrigger-type arms which are drilled and tapped to accept loading screws. These two screws, differentially-disposed, are used for torsional loading of the encasement by use of the torsion bar attachment.

An assembly sketch of the complete test unit comprising the strain-gage beam, the encasement and the test fixture is given in Figure 8. The test fixture is seen to be supported by an L-shaped frame (item -1). The pins in the base member of the frame were installed to act as guides and slide within the longitudinal slots of the bed assembly of the optical comparator. Thus the horizontal member of the frame is the reference surface against which the encasement deflections are measured. By attaching this reference structure directly to the encasement base, the effects of any relative deflections between the casement and the test fixture due to applied loads are eliminated.

Figure 9 is a photograph of the encasement assembled in the test fixture. The instrumented strain-gage beam is shown alongside the fixture.

3.3 STRAIN GAGE INSTRUMENTATION

Manufacturer's* recommended procedures and materials were used in the bonding of the SA-06-125AC-350 gages (see Section 2.5.1 for an explanation of the coding) to the beam. Each gage was trimmed in width to within 0.01 inch of the grid to fit the width of the beam. Also the front edge of each gage was trimmed to within 0.01 inch of the grid to permit placing the active area of the grid as close as possible to the zero-bending-moment point (for acceleration loading) of the beam (see Section 2.4.3). M-Bond 610 adhesive was employed since it is claimed* to provide thin glue lines free of voids and hence hydrostatic pressure effects. Only a single layer of a protective coating (M-Coat A) was applied to the strain gages in anticipation of possible needs to repair or replace the strain gage bridges (no such difficulties were experienced).

*Micro-Measurements, Romulus, Michigan 48174.

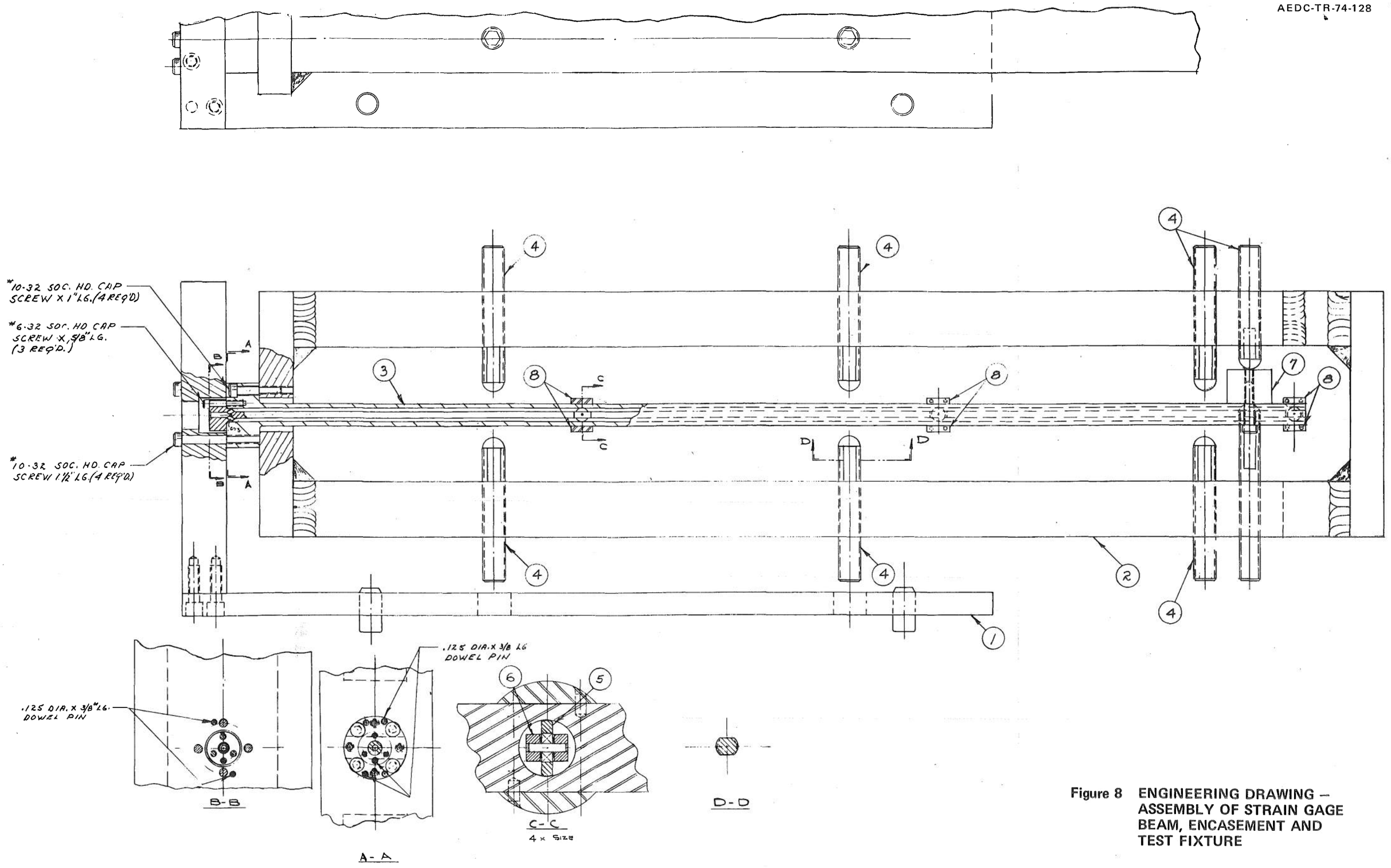

Figure 8 ENGINEERING DRAWING – ASSEMBLY OF STRAIN GAGE BEAM, ENCASEMENT AND TEST FIXTURE

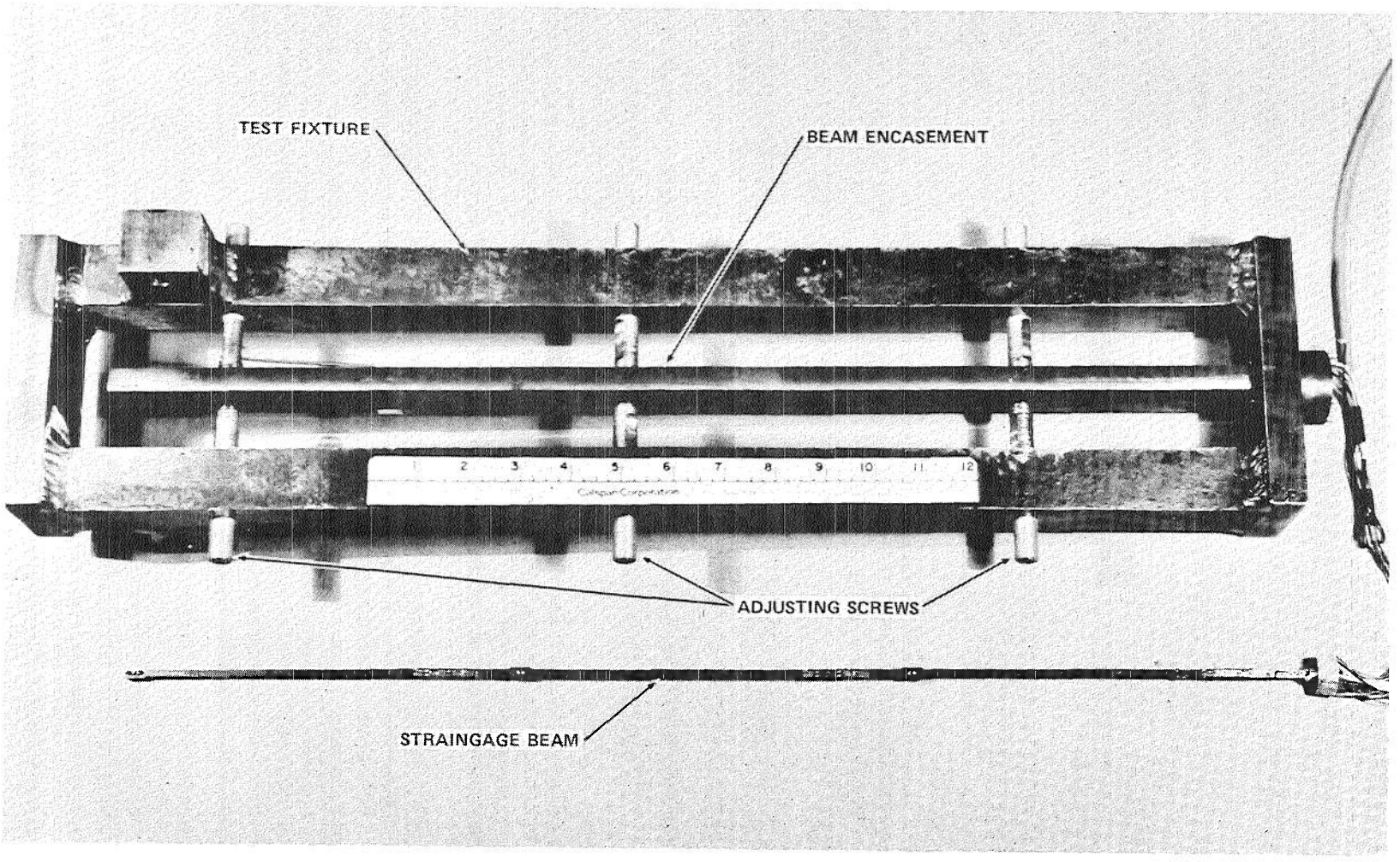

Figure 9 STRAIN GAGE BEAM, ENCASEMENT AND TEST FIXTURE

The gages were equipped with solder-dot terminals and separate, bondable terminal strips were used to anchor the lead wires. Small, strain-free loops of wire connected the gages and the terminal strips. Enamel-coated wires (to minimize wire diameter) from each bridge were carefully routed (and glued) along the beam. Lead wires generally followed the sides of the beam (and were glued thereto) to minimize any effect on bending stiffness of the beam. These lead wires terminated in additional (and larger) terminal strips on the base of the beam.

A six-wire type of strain gage wiring system was employed; two signal leads, two power leads and two leads for bridge calibration (shunt-type) (see Figure 6).

Electrical techniques were used to thermally compensate each bridge for stability of zero balance and sensitivity (span). The former used a series-type compensation by introducing temperature-sensitive wire (copper) and temperature-stable wire (manganin) in proper amounts and in the appropriate legs of the bridge. Similarly, span compensation was accomplished with nickel-foil resistors (bondable) which were placed in series with the power leads to each bridge. This compensation corrected for the variation of gage factor with temperature*.

Figure 10 is a photograph showing the details of the strain-gage installation on the beam. The gages, wire terminals and the span compensating resistor are clearly identifiable.

An analysis of the operational performance requirements of the electronic circuity to be used with the strain gages has been presented in Sections 2.5.2 and 2.6.2. In the bench tests intended to experimentally/ substantiate the validity of the analytical predictions, it is essential that the electronic hardware used is of a quality consistent with that assumed for analytical purposes. Since the program funding did not provide for the purchase of a high-quality, strain-gage electronic electronic readout system, it was necessary to improvise an equivalent quality system.

The Calspan Transonic Wind Tunnel Department has utilized strain gage type instrumentation for force and pressure measurements for many years. Consequently, they have developed very high quality electronic systems in support of their strain gage transducers. This in-house effort was undertaken at a time when suitable commercial equipment was not available. Since the current program did not involve dynamic testing, the static measurement capability was fully responsive to the needs of this program. A brief description of the apparatus follows.

*Time did not permit actual measurement of span variation with temperature so that the compensation was based on data on the variation of gage factor with temperature as supplied by the vendor.

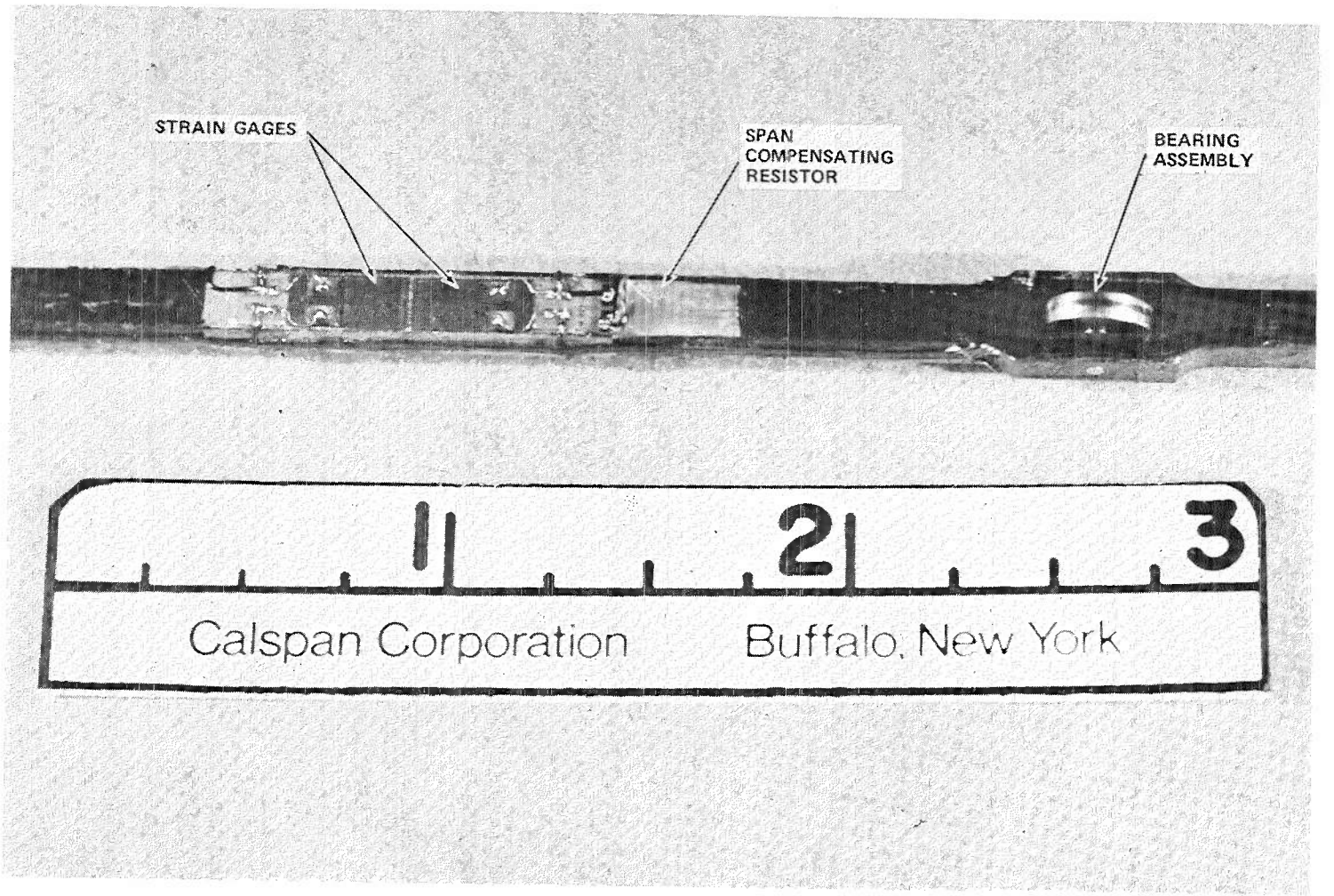

Figure 10 CLOSE-UP VIEW OF STRAIN GAGE INSTALLATION

The Calspan strain-gage readout equipment[6] is an all-electronic system with three channels per semi-portable rack. A 1kHz carrier system is employed with coherent detection of the bridge signal followed by a low-pass filter with a range of selectable time constants. A tuning fork stabilizes the carrier frequency permitting the use of an extremely narrow bandpass filter in the signal loop. All amplifiers use substantial amounts of negative feedback for very high stability in gain. The narrow bandwidth permits large gains to be achieved with excellent immunity to noise.

Each channel is complete with bridge balance controls, gain controls, filters and digital readouts. Power supply excitation is fixed at 3.5 volts rms (which is only about one half of the voltage rating of the strain gage bridges). Coarse and fine resistive balance controls are provided. A small oscilloscope is supplied with each channel and utilized in achieving an a-c balance of the bridge with a reactive (phasing) control in conjunction with a Lissajous pattern displayed on the scope. Three digits are displayed using neon tubes stacked in three adjacent columns. A panel light indicates whenever the display exceeds a count of 999. Full scale of the display is ±1999 counts with linearity and stability good to ±1 count. At maximum sensitivity, full scale is approximately equal to 300 microvolts and a measurement accuracy good to 1-2 microvolts. A second panel light designates strain polarity.

Provision is included for standardizing the sensitivity of each channel by the use of precision shunt resistor (also commonly called the dummy load resistor, DLR) across one arm of the bridge. By this means a known bridge unbalance is effected and the system gain may set to a pre-determined number of counts. In this manner the constancy of the system gain and calibration during the course of a test can be assured. For a four active-arm bridge of 350 ohms, full scale sensitivity corresponds to a strain of about 125 microstrain or a stress of 3750 psi in steel.*

A photograph of the readout equipment is shown in Figure 12.

3.4 ASSEMBLY

Only two portions of the assembly of the strain-gage beam and the encasement are critical and thus will be briefly described. One of these critical items is the assembly of the ball-bearing units. Because of their small size and the critical tolerances, care must be exercised not to distort the bearing when (1) the wheel assembly is fitted to the bearing periphery and (2) the shaft is fitted to the inner bearing diameter. This objective is accomplished by placing proper tolerances on both the wheel inner diameter and the shaft diameter. Care must also be exercised to maintain the bearings free

(6) 8-Foot Transonic Wind Tunnel, Calspan Report No. WTO-300, March 1968.

*Maximum calculated stresses in the beam at the instrumented locations are: 2,300, 8,200 and 19,200 psi.

of dirt. The bearings must not allow moments to be transmitted to the beam.

The insertion of the beam into the encasement is an operation that also requires care. Because the wheels on the bearings are fitted to the bore to tenths of a thousandths of an inch, it is essential that damage to the wheel peripheral surface of the bearings is avoided by using a light touch during assembly. A careful centering of the wheels within the bore must be maintained during insertion. On the initial assembly, intermittent and slight binding was noted as the beam was inserted and withdrawn from the encasement bore. Multiple passes through the bore were made with clean swabs to remove particulate matter adhering to the surfaces of the bore. These particles were presumed to be the result of carburizing of the contaminated bore surfaces (despite careful cleaning) during the heat-treat process.

After application of a coating of very light watch oil to the bore surfaces, the beam was more easily inserted into the bore. Because of the limberness of the beam and the close tolerances, a certain amount of "stiction" during assembly seems inevitable. It is recognized, of course, that the only critical part of the encasement/beam mating occurs when the bearing wheels are at their ultimate position in the bore. At this point, the system must be free of any binding.

Care also must be exercised in avoiding damage to the strain gages and the delicate electrical wiring during the assembly procedure.

3.5 TEST PROCEDURES

Following assembly of the test apparatus, this unit was placed on the optical comparator bed, as shown in the photograph of Figure 11, in preparation for the conduct of tests. The photograph clearly shows the three sighting segments on the upper surface* of the encasement which also has the torsion-loading bar attached near its free (left-hand) end.

Beam deflection data were obtained in the following manner. The unloaded position of the beam was taken as the reference against which subsequent measurements were made. Using the vernier, bed-elevating screw of the comparator, the screw-turns data corresponding to the height of the upper right corner of the upper segment and the lower left corner of the lower segment at each station along the encasement were recorded. The segments were viewed in profile on the comparator frosted viewing screen at an optical magnification of 50x which made possible readings repeatable to $\pm 1 \times 10^{-4}$ inch. It can be easily verified that the value obtained by taking one-half of the sum of these segment-pair readings yields the height of the center of the bearing shaft** (assuming the segments are accurately centered with respect to the bearing shaft). The profile view of the segment surface is aligned with respect to a

*Three segments are similarly disposed on the bottom surface.

**This is true also when the beam is deflected.

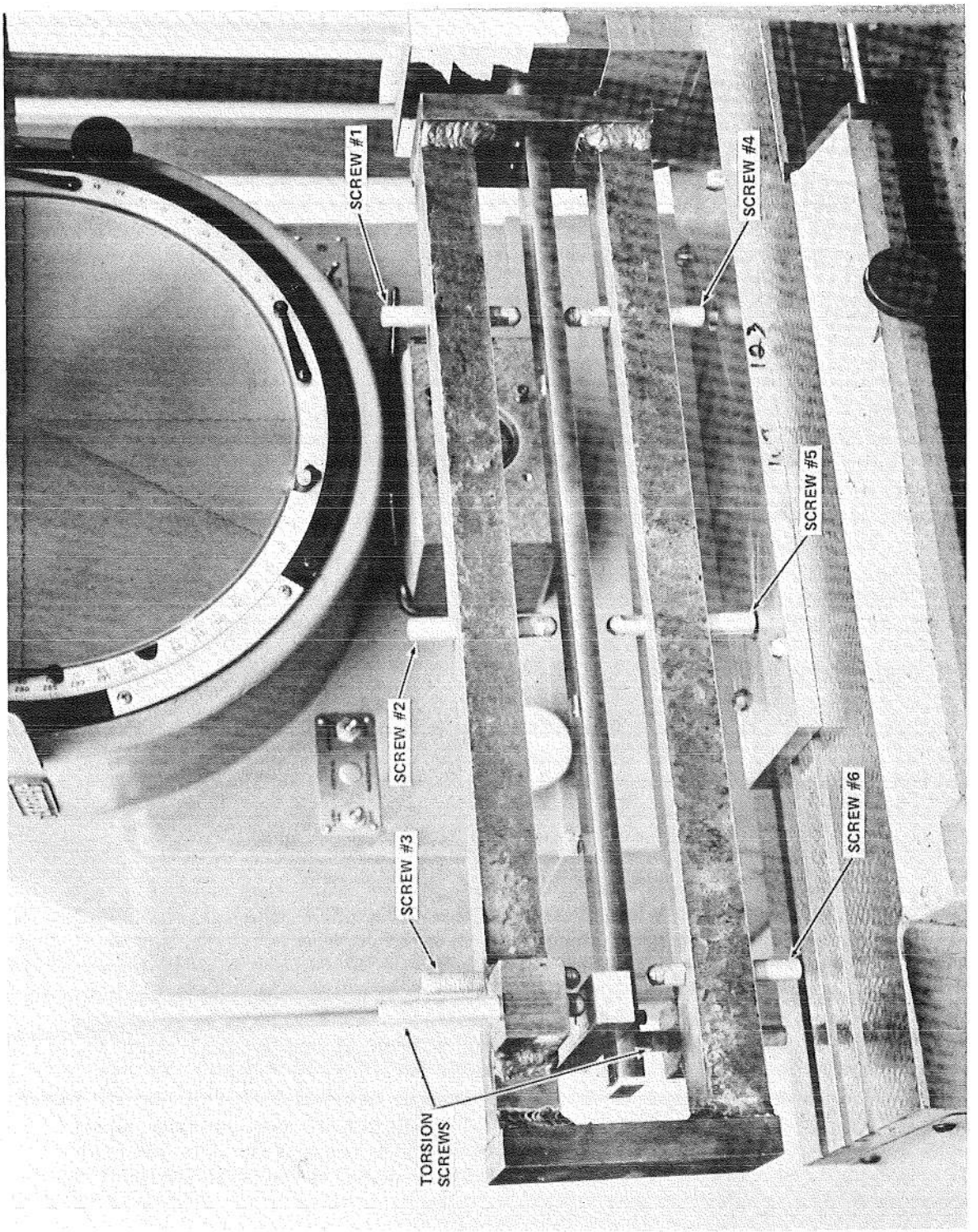

Figure 11 TEST APPARATUS ON OPTICAL COMPARATOR

reference line on the rotatable reticle of the viewing screen. Thus as the segments rotate* with beam deflection, the reference line is also rotated to be parallel with the segment surface to assure accurate measurements of the heights of the corners. Similarly, when the beam is deflected by the loading screws, the heights of the diagonal corners of each segment pair are measured. The actual beam deflection of each of the three reaction points is therefore obtained by subtracting the reference heights from their respective deflected heights. Beam deflections (and electrical outputs) are taken to be positive when the beam is deflected downward (reference Figure 11).

An overall view of the test set-up, including the three-channel strain-gage readout is shown in Figure 12. With the beam in the reference position (unloaded) each bridge was balanced (resistively and reactively) as indicated by a zero reading on the neon-tube digital displays. Thereafter the encasement was deflected to the approximate maximum levels expected at each of the three reaction points (y_1 = 0.036 inch, y_2 = 0.270 inch, y_3 = 1.00)** for an ATT-model wing. With the beam in this deflected position, the gains of the individual channels were adjusted to provide an electrical output of approximately 1500 counts. Best linearity is obtained from the electronic circuitry in this range. Thereafter, slight adjustments were made in gain so that the following conditions were satisfied.

CHANNEL	DLR	COUNTS
y_1	500k ohms	1550
y_2	160k ohms	1550
y_3	70k ohms	1550

By means of the above schedule, the gains of the individual channels could be precisely set during the course of the tests by periodic checks and making slight gain adjustments, if required. Gain checks and zero checks were made before and after each run.

Beam deflection data for the torsion tests were taken in the identical manner described above. A different procedure, described in Section 3.6.3, was used during the tests conducted at reduced temperatures.

3.6 ANALYSIS OF DATA

The experimental effort was designed to provide (1) beam deflection and electrical output data required to determine the coefficient matrix for Equation 7, (2) a comparision of measured with calculated deflections, (3) an assessment of torsion effects on deflection measurements and (4) an

*Relative to the horizontal.

**y_1 is the deflection of the reaction point nearest the fixed end of the beam.

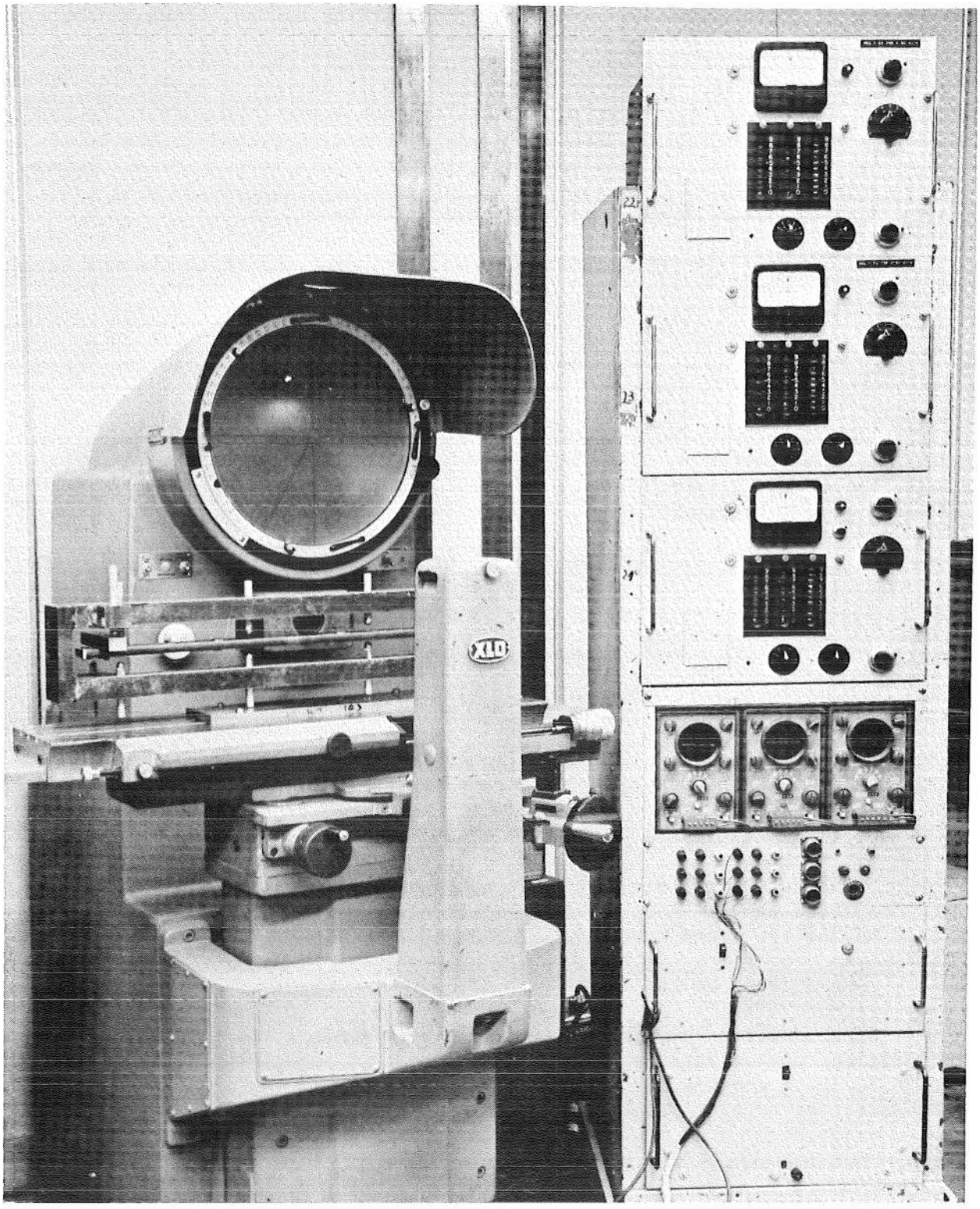

Figure 12 TEST CONFIGURATION INCLUDING ELECTRONIC READOUTS

evaluation of ambient temperature variations on system performance. Table 3 lists the schedule of test operations which were performed together with such other details as functional purpose, manner of loading, etc. An extremely tight time schedule and limited financial resources dictated both the size of the test program and its phasing. For example, the entire test sequence was completed before any computer feedback on data quality had become available.

As shown in Table 3, the bulk of the tests were made for the purpose of generating data for the coefficient matrix determination. These same data, of course, would serve the purpose of correlating calculated and measured deflections. In producing these data, the beam was loaded in an arbitrary manner without regard to actual shapes which might be assumed by a model wing

Table 3

SCHEDULE OF TEST OPERATIONS

RUN NO.	LOADING (SCREW #)	BEAM DEFLECTION (POLARITY)	PURPOSE	NO. TEST PTS.
1	3	+	A	8
2	2	+	A	7
3	1	+	A	6
4	1, 3, 5	+	A	13
5	3	+	B	6
6	6	–	A	5
7	5	–	A	6
8	4	–	A	5
9	2, 4, 6	–	A	17
10	1, 3, 5	+	C	8
11	1, 3, 4, 5	+	A*	10
12	3	+	D	7
13	3	+	D*	7
			TOTAL	105

KEY: A - MATRIX COEFFICIENT COMPUTATION
A* - SAME AS "A" ABOVE EXCEPT LARGE DEFLECTIONS
B - CALIBRATION OF SCREW #3
C - TORSION/DEFLECTION
D - TEMPERATURE TESTS (-8.5°F)
D* - SAME AS "D" ABOVE EXCEPT (-40.0°F)

under aerodynamic loading. Because of the cumbersome and time-consuming process by which the deflections were optically measured and the fact that a change in load at one screw position caused a change in deflection at all three reaction points, it was not practically feasible to attempt to duplicate wing bending shapes. Run No. 11 represents a very approximate approach to simulating loaded-wing shapes. It is to be noted, that there is no reason why wing bending shape should be duplicated to verify the strain-gage technique.

3.6.1 Measured Versus Calculated Deflections

The Calspan Transonic Wind Tunnel Department has a computer program used for the calculation of coefficient matrices, based on calibration data, for wind tunnel model force balances. This computer routine was adapted to the needs of this program. It provides a printout of the following data: (a) the matrix coefficients (b) the input data, (c) the calculated deflections, (d) the corresponding measured deflections, (e) the differences between measured and calculated values and (f) the standard deviation of the differences.

Matrix coefficients were determined from an input sample of 83 test points comprising Run Numbers 1 through 9 and 11. These input data consisted of measured values of the three deflections y_1, y_2, y_3 (in inches) and the corresponding strain-gage bridge output signals e_1, e_2, e_3 (in number of counts). These data resulted in the following matrix-form equation relating deflections and electrical outputs

$$\begin{bmatrix} y_1 \\ y_2 \\ y_3 \end{bmatrix} = \begin{bmatrix} 1.820 \times 10^{-5} & 1.325 \times 10^{-5} & -7.801 \times 10^{-6} \\ 4.555 \times 10^{-5} & 1.364 \times 10^{-4} & -1.497 \times 10^{-5} \\ 7.268 \times 10^{-5} & 2.888 \times 10^{-4} & 2.336 \times 10^{-4} \end{bmatrix} \begin{bmatrix} e_1 \\ e_2 \\ e_3 \end{bmatrix} \quad (8)$$

Using Equation (8), the measured electrical outputs were then used to compute the corresponding values of deflections. These were then compared with the deflections that were measured optically.

The computer routine also has a feature which permits setting an arbitrary tolerance on the discrepancy between a measured and a computed value. When this tolerance level is exceeded, that test point is "flagged" on the printout. A tolerance level of 2×10^{-3} inch was selected corresponding to a deflection error of approximately 0.05° for the dual-probe geometry analyzed in Section 2.0. Only one point* was thus flagged, exceeding the tolerance limit by two ten-thousandths of an inch. Likely, this was the result of a reading error.

Estimates of the standard deviations of the differences between computed and measured deflections were determined on the assumption that the errors followed a normal distribution. The following results were obtained.

*Out of a total of 249.

DEFLECTION STATION	STANDARD DEVIATION (inches)
y_1	0.0003
y_2	0.0005
y_3	0.0008

Thus the probability of a y_1 error exceeding 0.0009 inch, a y_2 error exceeding 0.0015 inch and a y_3 error exceeding 0.0024 inch is approximately 0.0026.

No evidence of hysteresis was noted upon removal of the load. Digital readouts returned to zero within ±1 count.

A complete tabulation of the test data is included in Appendix E which gives the measured and computed values of the deflections as well as the corresponding electrical outputs. Figure 13 consists of bar chart graphs showing the frequency distribution of the deflection errors in y_1, y_2 and y_3. The graphs indicate that the errors do tend to follow a Gaussian (normal) distribution.

3.6.2 Effects of Applied Torsion

Torsion tests were made at encasement twist angles of 1.4° and 2.75° and two different initial (no twist) loading conditions. The data are summarized in Appendix E as Run No. 10. A tabulation of the deflection errors is shown below as a function of twist angle (θ).

LOADING CONDITION 1

TWIST ANGLE, θ	y_1	y_2	y_3
0°*	0.0009 in.	0.0016 in.	0.0010 in.
1.4°	0.0013 in.	0.0025 in.	0.0023 in.
2.75°	0.0015 in.	0.0022 in.	0.0024 in.

LOADING CONDITION 2

0°*	0.0009 in.	0.0014 in.	0.0018 in.
1.40	0.0011 in.	0.0013 in.	0.0004 in.
2.75°	0.0012 in.	0.0029 in.	0.0005 in.

*Errors at 0° are averages of two test points

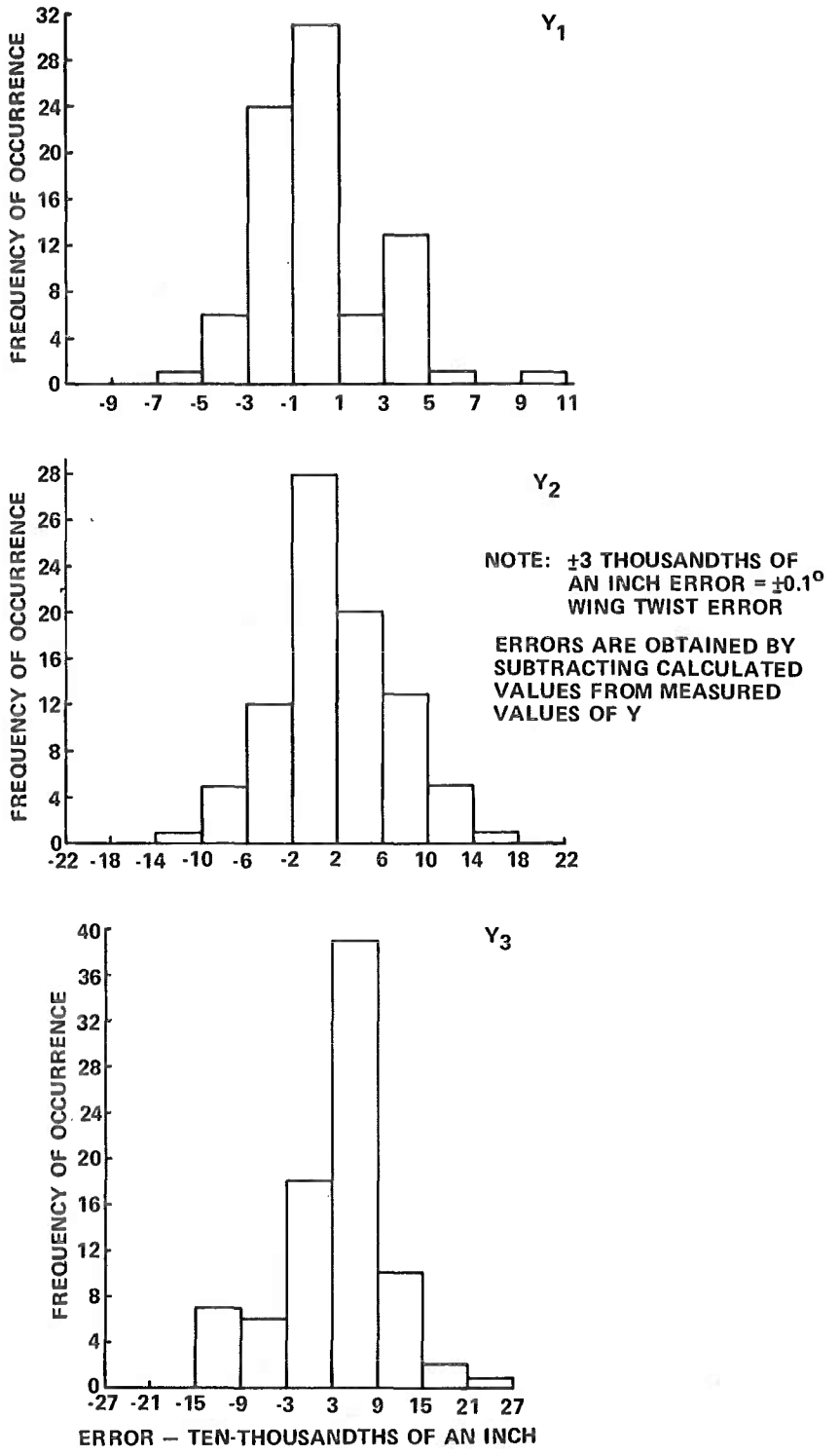

Figure 13 DEFLECTION ERRORS IN Y MEASUREMENT – SIMPLE BENDING TESTS AT ROOM TEMPERATURE

Several factors standout in these data: (1) the errors in most cases (especially in y_1 and y_2) are larger than normal*, (2) the errors at zero twist angle are unusually large, (3) the errors are of one polarity (the calculated value is consistently smaller than the measured value) and (4) there does not appear to be a consistent trend in the results as a function of twist angle.

One mitigating factor is the fact that the e_1 electronic channel developed a reactive (phase unbalance) during the course of these tests in the amount of 21 counts. From Equation (8), it can be shown that errors of approximately 0.4×10^{-3} inch in y_1 to 1.5×10^{-3} inch in y_3 will result from such a shift in count. At the time of these tests, the impact of such a shift in count was not appreciated and the tests were not repeated.

Despite the lack of consistency in the data, there is evidence of an interaction between the measured electrical outputs and the applied torsion load. The magnitude of such interaction is still small enough so that the tolerance band of 3×10^{-3} inch for the overall system has not been exceeded.

It is conceivable that the manner of applying the deflection/torsion loads could also produce different effects. For example, in the test conducted the beam was first deflected and then torsion applied since the design of the test fixture made this sequence convenient. It is also possible to first apply a torsion to the beam and then the deflection load or to apply both simultaneously as would occur in the wind tunnel situation. Further discussion on the torsion effects appears in subsequent sections of the report (Sections 3.7 and 3.8)

3.6.3 Effects of Variation in Ambient Temperature

The test fixture was not designed to permit a direct measure of the actual encasement deflection at reduced temperatures when the assembly was within the cold chamber. Rather, deflections were inferred from the room temperature calibration of one of the outboard loading screws (screw #3). The assumption was made that this calibration would hold, within narrow limits over the limited range of deflections imposed, at reduced temperatures.

The outboard screw was equipped with a long pointer which was set with reference to a metallic index tab attached to the encasement. Thus use of this screw was limited to a whole number of turns.** In use, this screw was rotated until positive contact with the encasement was established (as indicated by the presence of bridge electrical outputs). The pointer was then set with reference to the index mark, the strain-gage bridges electrically rebalanced and then the screw advanced by a whole number of turns. At room temperature (~76°F) the actual encasement deflections were measured optically (Run No. 5).

** One turn was equivalent to 50×10^{-3} inch.

* See Figure 13, for example.

Following this calibration and with the index screw returned to its reference setting (with a slight preload), the unit was installed in a cold chamber* where the screw was again advanced in the same manner as during calibration. A summary of the test data is shown in Table 4. It is seen that there are no apparent effects of temperature on the performance of the strain-gage probe. The differences are very small and reflect the precision of the mechanical system and the human operator. In two cases, sizable differences occur (one at room temperature) but these are probably human errors in data recording since they do not repeat. It is to be noted that the span (sensitivity) compensation was accomplished without actually subjecting the equipment to reduced temperatures to determine the temperature coefficient for each strain-gage bridge. Instead, the compensation was made solely on the basis of the data supplied by the vendor on the variation of gage factor with temperature. Since the variation of gage factor for Constantan gages is small (0.8% over a range from -100°F to -100°F), it would probably be unwarranted to generalize this experience to gages having a larger temperature sensitivity.

3.7 DISCUSSION OF RESULTS

The test data are considered to show a high degree of accuracy and precision in substantiating the feasibility of using the strain-gage probe technique for measuring model deformation in the HIRT environment. Further, it is felt the probe performance is even better than these data would indicate since the tests were conducted under circumstances which, in some cases, tended to compromise results. For example, the electronic readout system was designed to be operated from regulated a-c lines for achieving the ultimate stability. In using the optical comparator, it was necessary to conduct the tests in the machine shop area where line voltage regulation was quite poor. Manual control was exerted over the supply voltage to the readout system using a Variac transformer.

In addition, intermittent instability was noted in the e_3 readout unit during the earlier test runs. This difficulty was ultimately traced to faulty electrical connectors and corrected.

A minor factor, yet one that probably is detectable in view of the high degree of resolution in the measurement of deflection, is the truncation of the matrix coefficients in the computer program. While the calculation of the coefficients themselves was carried to more than four significant figures, the calculation of the deflections was made in some cases by truncating these coefficients to three figures. A check showed that the net effect amounted to one to two ten-thousandths of an inch only at large electrical outputs (counts). Time did not permit modifying the computer program to avoid such errors which were felt to be small enough to be acceptable.

As was noted earlier, the readout equipment supplied the strain gage bridges at approximately one half of the supply voltage which was assumed

*REVCO, Inc. Model SZH-653.

Table 4 DIFFERENCES BETWEEN MEASURED AND COMPUTED DEFLECTIONS AT THREE DIFFERENT AMBIENT TEMPERATURES

	ROOM TEMPERATURE (~ 75°F)		
SCREW TURNS	Y_1	Y_2	Y_3
1*	0.0001 IN.	0.0003 IN.	0.0014 IN.
2*	0.0001	-0.0001	0.0001
3*	0.0000	-0.0001	0.0002
4	0.0000	-0.0005	-0.0003
	-8.5 °F		
1*	0.0002 IN.	0.0004 IN.	-0.0017 IN.
2*	0.0002	0.0000	0.0001
3*	0.0002	0.0002	0.0001
4	0.0002	0.0001	-0.0001
	-40.0°F		
1*	0.0001 IN.	0.0001 IN.	0.0004 IN.
2*	0.0001	-0.0002	0.0000
3*	0.0000	-0.0001	0.0001
4	0.0001	-0.0002	-0.0003

*DATA FOR THESE SCREW SETTINGS ARE THE AVERAGE FOR TWO TESTS

in the Phase I analytical study. As a consequence, the signal-to-noise ratio of the system was not optimized.

The foregoing comments are offered to place these test data in a proper frame of reference and to indicate they represent a conservative indication of the strain-gage probe performance capability.

Deflection errors, as expressed in terms of standard deviation, increase in proceeding from y_1 to y_3.* Since most analog-type measurement transducers have an accuracy characterized by a percentage-of-full-scale figure (once favorable signal-to-noise ratios are realized), this result is not unexpected since $y_1 < y_2 < y_3$. In the test study, fixed gains were used in all three channels based on maximum ATT model wing deflections. In actual model testing in the wind tunnel one would set gains based on expected maximum deflections for each test rather than on maximum system capability. In this way, optimum signal-to-noise ratios would be obtained for each test.

A direct observation of the electronic readouts failed to show the presence of any hysteresis in the probe/encasement assembly. Removal of the deflecting loads would result in a prompt return of all three channels to a zero-count condition.** The test results also fail to indicate the existence of any significant mechanical "play" in the bearing assemblies.

Data at reduced temperatures do not show any significant or consistent thermal effects on probe performance. These data were taken at equilibrium conditions and do not take thermal transients into account. In view of the three-second test duration of HIRT, it is doubtful if any-thermal transients will be sensed by the strain-gage installations within the model wing.

Deflection errors appear to be affected by the presence of applied torsion to the beam/encasement assembly. Nevertheless, these errors still remain within acceptable tolerance. Unfortunately, the test results are few in number and do not indicate any consistent trends. Suggestions for further study of the effects of torsion are made in the next sections.

3.8 DESIGN EVALUATION

The purpose of this section is to offer a brief critique of the initial design concepts of the strain-gage probe technique based on the benefits of the experimental evaluation of the prototype unit. On an overall basis, the test results represent a gratifying verification of the soundness of the initial design concepts. Consequently, only minor recommendations in design modifications are offered.

---

* Section 3.6.1

** ±one count.

Assembly of the strain-gage beam into the encasement bore continually presented slight binding problems quite distinct from the initial difficulty with particulate matter in the bore. This binding is believed to be associated with the contour of the outer periphery of the bearing wheel which results in a wedging action whenever a slight misalignment of the wheel in the bore occurs. The accompanying sketch illustrates the prototype design and the recommended modification. It is seen that in the original design the bearing wheel makes contact with the bore wall only at the point of the maximum wheel diameter. The recommended design features a flat-top wheel with contact on the bore wall occurring at two points on the wheel. Wedging of the wheel in the bore is expected to be alleviated by the modified design.

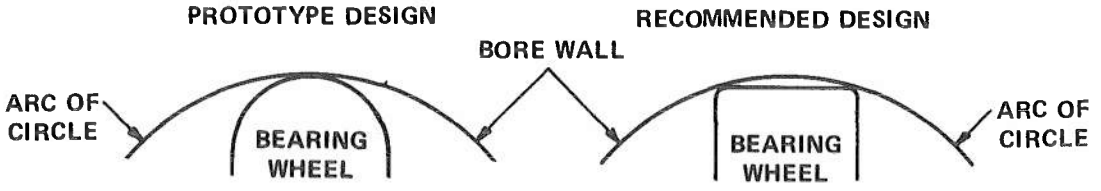

As regards the effects of torsion, it is felt that the source of interaction between deflection and torsion should be isolated. This could be done by removing the strain-gage beam from the encasement and subjecting it to a purely torsional load and noting the electrical outputs of the three strain gage bridges. It is possible that one (or two) of the bridges may show a sensitivity to torsional strains.* If this is the case, then the matter of gage geometrical alignment will need to be studied as a possible source of torsional sensitivity. If such an approach does not yield any resolution, then internal compensation for torsion is possible. Strain gages may be installed which sense only torsional strains and their electrical outputs properly combined with the normal strain-gage outputs to "null" signals due to torsion loads.

*Most strain gages exhibit some sensitivity to transverse strains. For Constantan metal-foil gages this sensitivity is normally very small.

Section 4.0
CONCLUSIONS AND RECOMMENDATIONS

The analytical studies and the subsequent experimental test program have both shown that a strain-gage probe represents a viable, on-board sensor that can be installed in a wind tunnel model to measure model deformation to the desired degree of accuracy in the HIRT operating environment. A dual-probe geometry permits measurement of wing twist to better than ±0.1 degree and wing deflections to much better (less than 3×10^{-3} inch) than the 50×10^{-3} inch objective. It was demonstrated that adequate temperature compensation of the probe is possible so that only a room-temperature calibration of the system is required for operation at temperatures as low as -60°F.

There are no fundamental limitations in the low frequency response capability of the probe sensor which limit its application to test durations typified by Ludwieg tube test facilities. Thus the probe could be used in continuous-running wind tunnels as well.

Based on a survey of available instrumentation and model spatial limitations, it was concluded that a 0.1-degree accuracy in determining model pitch could be achieved using an on-board linear accelerometer and a rate gyro in combination.

Dynamic response aspects of the model deformation measuring probe were only explored analytically and requirements for the electronic data conditioning were specified. It was determined that the system was capable of accurately following a low-amplitude oscillation of the model at a frequency of 50 Hz.

It is recommended that further experimental tests be devoted to the resolution of torsion effects on the strain-gage probe following the procedures outlined in Section 3.8. Additionally, an experimental verification should be made of the dynamic characteristics of the probe sensor and the effects of acceleration forces. Ultimately, a dual-probe system should be built, installed in a real (or simulated) model wing and its performance evaluated.

Assembly of the strain-gage beam into the encasement bore continually presented slight binding problems quite distinct from the initial difficulty with particulate matter in the bore. This binding is believed to be associated with the contour of the outer periphery of the bearing wheel which results in a wedging action whenever a slight misalignment of the wheel in the bore occurs. The accompanying sketch illustrates the prototype design and the recommended modification. It is seen that in the original design the bearing wheel makes contact with the bore wall only at the point of the maximum wheel diameter. The recommended design features a flat-top wheel with contact on the bore wall occurring at two points on the wheel. Wedging of the wheel in the bore is expected to be alleviated by the modified design.

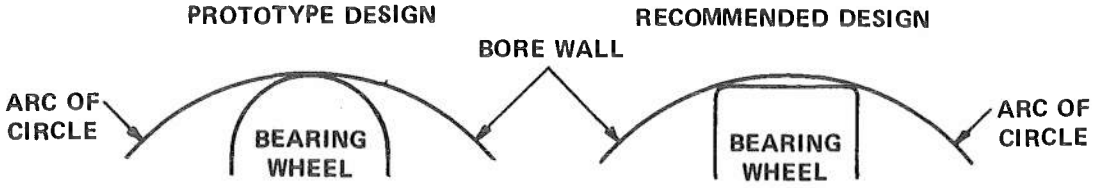

As regards the effects of torsion, it is felt that the source of interaction between deflection and torsion should be isolated. This could be done by removing the strain-gage beam from the encasement and subjecting it to a purely torsional load and noting the electrical outputs of the three strain gage bridges. It is possible that one (or two) of the bridges may show a sensitivity to torsional strains.* If this is the case, then the matter of gage geometrical alignment will need to be studied as a possible source of torsional sensitivity. If such an approach does not yield any resolution, then internal compensation for torsion is possible. Strain gages may be installed which sense only torsional strains and their electrical outputs properly combined with the normal strain-gage outputs to "null" signals due to torsion loads.

*Most strain gages exhibit some sensitivity to transverse strains. For Constantan metal-foil gages this sensitivity is normally very small.

In the above expression, R and L correspond, respectively, to the initial resistance and length of the gage while ΔR and ΔL are the incremental changes in resistance and length produced by the strain in the surface to which the gage is attached. The gage factor is a measure of gage sensitivity, the higher the gage factor the larger the change in gage resistance per unit strain.

The wire employed in a strain gage should be characterized by a high specific resistivity, a large change in resistance with strain, a high elastic limit and electrical and mechanical properties which are independent of temperature. Additionally, the change in gage resistance should be a linear function of strain. Wire materials satisfying all of these criteria just do not exist. The most commonly used materials, which represent a satisfactory compromise, are a 0.60/0.40 alloy of nickel/copper which is commonly known as Constantan and a 0.45/0.55 alloy called Advance. To increase gage resistance and to insure that the adhesive used to bond the gage is stronger than the wire, the wire diameter is very small (typically, about one mil or less).

The basic strain gage takes the form of a grid comprised of a series of long parallel loops. This grid is typically cemented between two pieces of a thin material (paper, plastic, etc.) which serves to provide mechanical protection for the fragile gage and also to electrically insulate it from any conductors to which it may be attached.

Specific features which have contributed to the universal acceptance of bonded resistance strain gages are tabulated below:

- small size
- light weight and ruggedness
- ease of attachment and mounting
- low cost

- excellent electrical stability
- low impedance (resulting in low susceptability to noise pickup)
- operable on a-c or d-c excitation
- readily temperature compensated
- good high frequency response for dynamic stress studies

If there is one area in which the resistance strain gage can be faulted it is in regard to its low sensitivity. For wire or metallic gages, the maximum change in resistance experienced is typically about one per cent of the basic gage resistance. As discussed subsequently, simple, yet sensitive, electrical circuits are available to accommodate this situation.

Virtually all of the older variety of strain gages were made of wire of a small and uniform diameter. As a result, the wire sensing elements present a small surface area to the specimen. These gages have gage factors in the approximate range from 2 to 5 and resistances in the range from 50 to 100 ohms.

With the development of modern photo-etching techniques, the metallic foil gage came into prominence and has largely displaced the wire gage in most applications. Using this technique very intricate grid patterns can be precisely achieved by etching thin sheets (usually less than 2×10^{-4} inches thick) of heat-treated metallic alloys. These foil elements have a large ratio of surface area to cross-sectional area as compared to wire gages (see Figure 1). This feature produces improved stability under sustained loading and temperature extremes. Also, the combination of a large surface and thin cross section minimizes temperature differences between the gage and the specimen. Dissipation of gage heating due to the excitation current is thereby facilitated. An additional advantage of the foil gage is the improved adhesion to the specimen as the result of the large surface area.

While strain gages are available in many configurations, the most popular is that designed to measure uniaxial strains. In this configuration the greatest length of strain-sensing material is placed in the direction of the strain being measured (Figure A-1). Nevertheless, the end loops or tabs of the gage result in a transverse strain sensitivity of the gage. By providing a capability to enlarge the cross-sectional area of the end loops, the foil gage achieves a lower sensitivity to transverse strains than is possible with a wire gage.

Resistance ranges for wire and foil gages are nominally the same, however foil gages are available in much smaller sizes than wire gages. The former are available in length/width dimensions as small as 0.015 in./0.020 in. while the latter are more of the order of 0.125 in./0.187 in.

A third variety of strain gage that has recently become available is the semiconductor type. The material used in fabricating these gages is a specially-grown silicon crystal doped with a controlled impurity content to obtain specific electrical characteristics. This crystal is cut into filaments which exhibit the property of peizoresistivity, that is, a change in resistivity with applied strain. Depending on the orientation of the crystallographic axis relative to the cut of the filament, the change in resistance with strain may be either positive or negative.

Compared to the wire and foil gages, the semiconductor gage is characterized by the following factors:

- much higher sensitivity (gage factors range between 45 and 200)
- higher resistance range (typically 60 ohms to 10,000 ohms)
- longer fatigue life
- lower hysteresis
- sizes equivalent to foil gages
- very low thermal coefficient of expansion ($\simeq$2.5 ppm/^{o}F)

The increased sensitivity of the semi-conductor strain gage is, however, coupled with corresponding increases in the effects of ambient temperature and a nonlinearity of output with strain. As a consequence, the major utility of these gages is in high-output transducers wherein electrical compensation can be incorporated into the circuitry to minimize the effects of temperature on sensitivity and nonlinearity. The low expansion coefficient of the gage relative to that of most metals, results in large "apparent" strains as the result of the differential expansion with temperature. In general, the semiconductor is not normally used in stress analysis unless the increased sensitivity is critical to the needs of the task.

GAGE CIRCUITS

A bridge-type electrical circuit, Figure A-2, is commonly used with all types of strain gages since it permits the strain-induced resistance changes of the gages to be measured more accurately and more directly than by conventional electrical instruments. Bridge circuits can be synthesized using either one, two or four active gages. Active gages are those subjected to strain and contrast with dummy gages which are located adjacent to the active gages but in a strain-free environment. These dummy gages are employed to provide compensation for thermal effects.

Optimum sensitivity and thermal compensation is achieved if all four arms of the bridge are active gages. In such a situation, the adjacent arms of the bridge are so arranged that their resistance changes (ΔR) are equal and of opposite sign. Accordingly, R_1 and R_4 of Figure 2 might be in tension while R_2 and R_3 would be in compression. For the special case where $R_1 = R_2 = R_3 = R_4 = R$, the following relation applies:

$$\frac{E_{out}^{*}}{E_{in}} = \frac{\Delta R}{R} \qquad (A-2)$$

*E_{out} is the open circuit voltage.

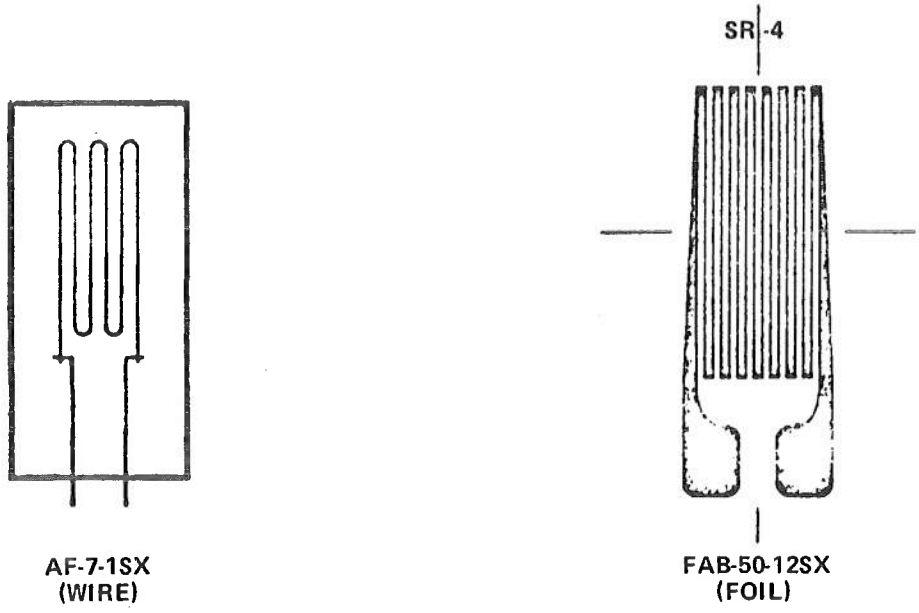

Figure A-1 UNIAXIAL STRAIN GAGES

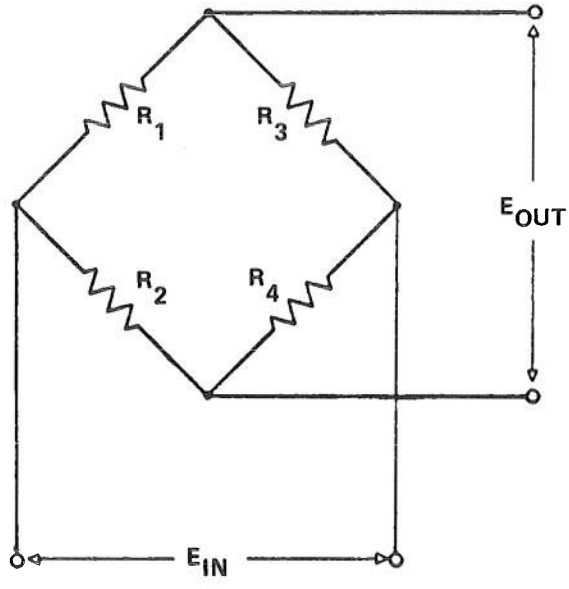

Figure A-2 WHEATSTONE BRIDGE CIRCUIT

Thus a voltage output linear with the applied strain is obtained provided the gage factor remains constant (E_{out} is also presumed to be constant). Bridge voltage supply may be a.c. or d.c., constant voltage or constant current. Since the output signal is proportional to the input voltage, the tendency is to use maximum permissible supply voltage. High gage currents produce gage heating which affects the zero-strain stability of the bridge and the thermal compensation in an adverse manner. Permissible wattage density data for various gages bonded to different materials are provided by the strain gage manufacturer. For optimum results in critical applications, the minimum gage current consistent with a satisfactory signal-to-noise ratio should be used.

The bridge circuit of Figure A-2 is only conceptual to the extent that no provision is shown for balancing (zeroing) the circuit precisely or providing necessary compensation. A more realistic circuit is discussed in the following section.

PRACTICAL CONSIDERATIONS

The disarmingly simple nature of the strain gage and its associated electrical circuit belie the subtle and complex difficulties that confront the unwary user who attempts to realize measurements that are precise and accurate. In the following paragraphs some of important aspects of practical applications are considered for the case of a four active-arm bridge circuit (special precautions pertain to configurations comprising one or two active arms).

a. Installation

The location selected for the placement of strain gages must consider the avoidance of the undesirable effects of temperature variations (gradients), stress concentrations and local buckling. It is desirable that the installation

of the gages subjects them to a single type loading (bending, axial, etc.). All gages plus any compensatory resistances must be so placed as to minimize the existance of temperature gradients.

Modern foil gages are available in a fully encapsulated state to provide protection from the harmful effects of moisture and humidity which can produce electrical leakage. Special materials for over-coating the gages are available which provide moisture proofing and in addition offer thermal insulation from drafts and spurious thermal disturbances.

The performance and stability of the gages is critically dependent on the quality of the bond with the structural member. Instructions furnished by the manufacturer must be scrupulously observed. For extreme conditions of ambient temperature and pressure (above and below atmospheric), special adhesives are available and should be used. For example, void-free adhesives are supplied for bonding gages which must operate at very high or very low pressures.

b. Electrical

The minimal detectable strain that can be detected by the strain gage bridge is dependent upon the noise level of the circuit. This noise level includes the fineness of the bridge balance and any spurious signals induced into the bridge or connecting lead wires. With d-c excitation, bridge balance is purely resistive while with a-c excitation both the resistive and reactive components must be carefully balanced. For this reason, d-c excitation is often used especially where the dynamic content of the signal is broadband and would require a high frequency a-c carrier.

A constant voltage source is commonly used to excite the strain gage bridge. In this case the use of very long lead wires to the bridge could produce

a change in sensitivity with a change in temperature (due to the change in lead wire resistance). In situ calibration for such effects can be made by introducing a known resistance change in one of the legs of the bridge and noting the corresponding signal output.

In high vibration environments, electrical noise may be generated by the flexing of electrical cables. For such applications, a multiply-shielded, special low-noise cable is available.

Reference to the need to minimize gage self-heating by the bridge excitation has been cited earlier. As was noted, the construction of the foil gage is such that self-heating, as compared to the wire and semiconductor gages, is substantially reduced at a given power density input.

The physical details of the manner in which electrical leads are attached can also affect the accuracy of the resultant strain data. These leads must be attached so that no spurious strains are introduced as the result of unwanted tension in the leads. Generally the solution is to properly anchor the lead wires and utilize strain-relieving loops where differential motion between components is unavoidable.

c. Thermal

Ambient temperature variations potentially constitute one of the major sources of error in strain gage installations unless proper precautions are taken to minimize and/or compensate for the thermal effects. The gage installation and location details are important factors in the reduction of thermal problems. Recommended practice includes: symmetrical disposition of gages on the structure, selection of gage locations conducive to minimizing thermal gradients, use of

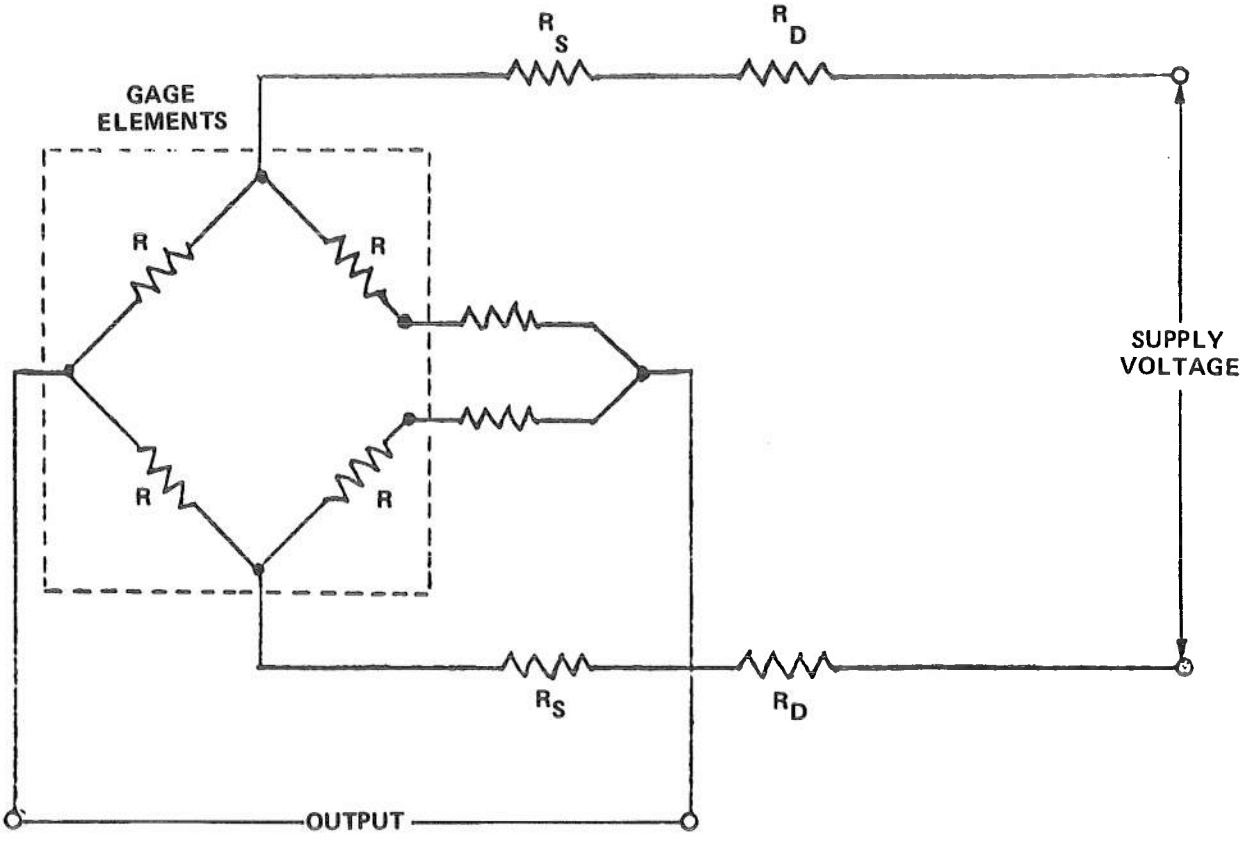

R = STRAIN GAGE
R_o = BRIDGE BALANCE RESISTOR
R_T = TEMPERATURE COMPENSATING RESISTOR (BALANCE)
R_S = TEMPERATURE COMPENSATING RESISTOR (SPAN)
R_D = VOLTAGE DROPPING RESISTOR

Figure A-3 TYPICAL COMPENSATED STRAIN GAGE BRIDGE CIRCUIT IN A TRANSDUCER APPLICATION

thermal insulation coatings on the gages and the placement of the complete bridge at the location of the strain to be measured.

The two principal temperature dependent properties of all strain gages (metal and semiconductor) are (1) the gage resistance and (2) the gage factor.* For metal gages, the temperature coefficient of resistance of the alloys used is very small and the net effect of temperature changes is to disturb the zero balance of the bridge. By selecting bridge gages from a given production lot, gage-to-gage differences can be minimized. A third factor is the difference in the thermal coefficient of expansion between the gage material and the structural member that results in apparent strains as temperature changes. Self-compensating strain gages (metal) are available which exhibit a very low temperature sensitivity when attached to the specific material (aluminum or steel) for which the gage has been designed.

A fourth factor is the change in elasticity or spring constant of the structural member with ambient temperature. Typically the temperature coefficient of Young's modulus of elasticity is -2 to -6 x 10^{-4} per °C. for most metals. The net effect is to change the calibration of the bridge circuit (applied load or deflection versus bridge output) as temperature changes. One gage manufacturer** currently supplies special metal-foil gages compensated for temperature effects that result in apparent strain and changes in Young's modulus when applied to 714 PH stainless steel (compensation is useful to -100°F). It is also feasible to use a compensated bridge circuit to correct for modulus changes by the use of a temperature-sensitive resistor in series with the bridge supply to suitably vary bridge excitation current. A fully-compensated bridge circuit is shown in Figure A-3.

*These variations are usually much larger for semiconductor gages.
**Micro-Measurements, Romulus, Michigan

In Figure A-3 the resistor R_s is a temperature-sensitive resistor which controls the bridge output (span) in a manner that compensates for the variation of Young's modulus of the spring material. The resistor thermal characteristics must be appropriate to the characteristics of the spring material used. The resistor R_T is also a temperature sensitive resistor used to maintain the zero-input, null balance of the bridge. Its position in the circuit must be determined by trial.

Since the schematic of Figure A-3 is for a transducer application, the several compensatory resistors are shown as being fixed. In experimental work, these would often be variable or adjustable resistances to provide flexibility. It is common practice to physically split or divide some of the compensating resistances since better thermal compensation results.

Typically, strain gages are designed for normal operation over the range from -100°F to 350°F. Special gages are available for short-term use outside this range.

d. Pressure

The possibility of pressure effects on strain gages subjected to pressures of 800 psia was considered insofar as spurious electrical signals might be produced. Two separate sources of difficulty may be encountered (1) an inherent pressure effect on the gage itself and (2) pressure effects due to voids in the glue line between the gage and its substrate. Data related to the former were found in the literature[1-3] and stated to be approximately -3 microstrain per 1000 psi. With a four-arm bridge configuration, the pressure effect will be cancelled electrically to the extent the pressure sensitivity of the gages used is identical. The latter item, related to voids, is a gage application problem and was discussed with a strain gage (metal foil) manufacturer[4]. It was stated that special adhesive materials

are available for bonding gages which preclude void formation in the glue line.

To summarize, the strain-gage technology currently available appears to be adequate to permit the successful measurement of model deformations in the environment of the HIRT test section. Careful and judicious engineering practice, born of practical experience with unusual and demanding strain gage applications, will be essential in developing the instrumentation hardware.

REFERENCES

1. Milligan, R.V., "Gross Hydrostatic Pressure Effects as Related to Foil and Wire Strain Gages," Experimental Mechanics, Vol. 7, No. 2., Feb. 1967, pp. 67-74.

2. Milligan, R.V., "Effects of High Pressure on Foil Strain Gages on Concave and Convex Surfaces," Experimental Mechanics, Vol. 5, No. 2, pp. 59-64.

3. Gerdeen, J.C., "Effects of Pressure on Small Foil Strain Gages," Experimental Mechanics, Vol. 3., No. 3, March 1963, pp. 73-80.

4. Telecon J. Raudenbush, Micro-Measurements Corporation, August 8, 1973.

BIBLIOGRAPHY

1. Catalog and Technical Data Binder, Micromeasurements, Romulus, Michigan 48174.

2. Kulit Semiconductor Strain Gages, Bulletin KSG-4, Kulite Semiconductor Products, Inc., Ridgefield, New Jersey 07657.

3. SR-4 Strain Gage Handbook, Volume I, BLH Electronics, Inc., Waltham, Massachusetts 02154.

4. Perry, C.C. and Lissner, H.R., The Strain Gage Primer (McGraw-Hill, 1955).

Appendix B

COMPUTATION OF BEAM DEFLECTION ERRORS RESULTING FROM ELECTRICAL NOISE

The evaluation of the feasibility of the strain gage probe, in part, requires the conversion of estimated levels of electrical noise into equivalent "noise" in the determination of beam deflections. This appendix outlines such a methodology.

In matrix form, the equations relating deflection (y) to moments (M) for a 0.15-inch square cross section beam are given below.

$$\begin{bmatrix} y_1 \\ y_2 \\ y_3 \end{bmatrix} = \frac{21.88}{EI} \begin{bmatrix} 1.2387 & 0.2841 & -0.0769 \\ 3.0968 & 2.878 & -0.1596 \\ 4.9550 & 6.0914 & 2.0676 \end{bmatrix} \begin{bmatrix} M_1 \\ M_2 \\ M_3 \end{bmatrix} \tag{B-1}$$

Beam strain (ε) may be substituted for the bending moment by the use of the following relation.

$$M = \frac{EI}{\mathcal{Z}} \varepsilon \tag{B-2}$$

where

E = beam modulus of elasticity (3×10^7 psi)

I = beam moment of inertia (4.219×10^{-5} in.$^{-4}$)

$\mathcal{Z}$ = one half beam thickness (7.50×10^{-2} in.)

Therefore Equation B-1 may be written as follows:

$$\begin{bmatrix} y_1 \\ y_2 \\ y_3 \end{bmatrix} 2.918 \times 10^{-4} \begin{bmatrix} 1.2387 & 0.2841 & -0.0769 \\ 3.0968 & 2.878 & -0.1596 \\ 4.9550 & 6.0914 & 2.0676 \end{bmatrix} \begin{bmatrix} \varepsilon_1 \\ \varepsilon_2 \\ \varepsilon_3 \end{bmatrix} \tag{B-3}$$

where ε is in microstrain units.

Writing out the three linear equations for y_1, y_2, y_3 in terms of ε_1, ε_2, ε_3 and deriving the total differential for each, the factors Δy_1, Δy_2, Δy_3 are obtained as functions of $\Delta\varepsilon_1$, $\Delta\varepsilon_2$, $\Delta\varepsilon_3$ where the Δ -quantities represent the error terms. Estimated values for $\Delta\varepsilon$ are based on system noise levels from such sources as amplifiers, for example, for which the following relation applies

$$\frac{\Delta \epsilon_1}{\epsilon_1} = \frac{\Delta V_1}{V_1} \qquad \text{(B-4)}$$

where V_1 is the strain-gage signal corresponding to ϵ_1 and ΔV_1 is the amplifier noise level. In like manner $\Delta \epsilon_2$ and $\Delta \epsilon_3$ can be determined and hence values for Δy_1, Δy_2, Δy_3.

A simple summation of the $\Delta \epsilon$ errors will yield a maximum possible value for Δy. Since the errors due to noise tend to be random type errors, the calculation of a root-sum-square value for Δy will provide a more probable value. This figure is obtained by taking the square root of the sums of the squares of the contributing $\Delta \epsilon$ values as per Equation B-3.

Appendix C
CALCULATION OF AMPLIFIER BANDWIDTH REQUIREMENTS

This appendix presents the methodology used in the calculation of the bandwidth requirements of an amplifier to minimize the time lag in response to a 50 Hz signal to acceptable levels. The criterion to be met is that the amplitude error in the output signal shall not exceed by 1×10^{-3} inch the instantaneous value of the input signal which has a frequency (maximum) of 50 Hz and a half-amplitude of 0.02 inch.

The input signal may be represented as

$$Y = A \sin \omega t \tag{C-1}$$

where Y = instantaneous amplitude, A = peak value of the input, ω = angular frequency, t = time. Differentiating Eq. C-1, one obtains the relation between amplitude error, ΔY, and a time lag, Δt.

$$\Delta Y = A \omega \cos \omega t \, \Delta t \tag{C-2}$$

Therefore $\Delta Y_{max} = A\omega\Delta t$. Substituting the proper numerical values, Δt is found to have a maximum permissible value of 1.59×10^{-4} second. Expressed as a phase lag, this figure is equivalent to 2.86 degrees.

Assume that the high frequency roll-off of the amplifier is representative of a first order, low-pass, RC filter as schematically shown below.

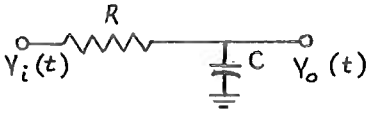

the transfer function for this network may be written as

$$\frac{Y_o(t)}{Y_i(t)} = \frac{1 - j\omega\tau}{1 + \omega^2\tau^2} \tag{C-3}$$

where τ = RC. The phase angle, ϕ, is given by the following equation

$$\tan \phi = -\omega\tau \tag{C-4}$$

Substituting ϕ = 2.86 degrees and $\omega = 100\pi$ into Eq. C-4, the value of the required network (amplifier) time constant can be found. Since the corner frequency, f_c, of a network, expressed in terms of its time constant is

$$f_c = \frac{1}{2\pi\tau} ,$$

the substitution of the value for τ yields a value of 1000 Hz for f_c.

The absolute magnitude of the output-input function, as obtained for Eq. C-3, is shown below.

$$\frac{|Y_o(t)|}{|Y_i(t)|} = \left[\frac{1+(\omega\tau)^2}{(1+\omega^2\tau^2)^2}\right]^{1/2} \qquad \text{(C-5)}$$

Evaluation of Eq. C-5 yields a value of 0.999 at a frequency of 50 Hz.

Appendix D
EVALUATION OF MODEL POSITION INDICATOR SYSTEMS

INTRODUCTION

The following material constitutes an evaluation of candidate devices or systems used to measure model pitch motions which can be related to angle of attack. The basic requirements are:

a) Model max pitch rate: 7°/sec

b) Model angle of attack range: -10 to +20°

c) Space available within model 6" dia by 11" long cavity

d) Pressure: 800 psia decreasing to 500 psia in 1/2 second

e) Temperature: -30°F decreasing to -60°F in 1/2 second

f) Accuracy ±0.1 degrees

As a first step in evaluating candidate devices, discussions were held with wind tunnel engineers from various companies to identify current techniques for measuring the model pitch angle. It appears that there is no standardized technique that is used. For example, Calspan employs bubble devices to set the model to various fixed pitch angles, but does not make dynamic measurements.

McDonnell Douglas uses a potentiometer pickoff located on the actuator controlling the pitch angle of the model. This arrangement does not have the desired accuracy or resolution especially in the typical vibration environment of model testing.

General Dynamics has used a pendulous device with some success; however, accuracy and resolution are compromised by vibration.

NASA-Langley has been using a pendulum-type linear accelerometer with good results although their tests have not been at 800 psia or at -60°F.

Several wind tunnel engineers expressed the desirability of having a better measurement system than is presently available.

DISCUSSION OF SUITABLE DEVICES

A number of devices could be used for this application; however, some have serious drawbacks such as excessive size and weight. The devices considered as possible candidates are:

1. Small displacement gyroscope
2. Rate gyroscope with external integrator
3. Linear accelerometer
4. Combination package of rate gyroscope and linear accelerometer.

Table D-1 summarizes characteristics of typical sensor types noted above. These characteristics are representative of the smallest and most accurate devices obtainable today. It should be noted that none of these devices could be used for the HIRT application without protecting them from the 800 psia wind tunnel pressure environment.

Displacement Gyro

The displacement gyro is attractive from the viewpoint of providing both static and dynamic pitch information directly; however, its size would require a relatively large pressure chamber which would make its installation in the model difficult. Figure D-1 shows typical electronic circuits required to process the attitude gyro sensor outputs.

Some additional advantages and disadvantages in using a displacement gyro are:

Advantages:

1) Static and dynamic pitch data for the model are available directly as analog voltages at the output of the sine θ to θ function generator module.

2) Roll angle measurement is available at very little extra cost since attitude gyros are designed to provide both pitch and roll outputs.

3) Attitude gyros are relatively insensitive to shock and vibration (compared to linear accelerometers or rate gyros).

Disadvantages:

1) The size and weight of an attitude gyro makes installation in a wind tunnel model difficult, particularly since the gyro must be installed in a container for protection from the high air pressure environment (800 psia).

2) Attitude gyros are expensive (five to ten times as much as a rate gyro or linear accelerometer).

Table D-1

TYPICAL SENSOR CHARACTERISTICS

SENSOR TYPE	MFG. & MODEL	RANGE	SIZE & WEIGHT	ACCURACY (REPEATABILITY TO ESTABLISHED VERTICAL)	GYRO COST	OPERATING LIFE
DISPLACEMENT GYRO	KEARFOTT C70-4130	PITCH ±82° ROLL 360°	3 11/64" SQ x 3.80" HIGH WT = 3.5 LB	±.5° to ±1.0°	$3500	1000 HRS MINIMUM
DISPLACEMENT GYRO	LEAR-SIEGLER 9000C	PITCH ±82° ROLL 360°	4" x 4" x 6" 3.0 LB	±.25° to ±.5°	$2600	1000 HRS MINIMUM
DISPLACEMENT GYRO	MINNEAPOLIS HONEYWELL GG99	PITCH ±82° ROLL 360°	4" x 4" x 6" LG 4.0 LB	±.15° to ±.2°	$10,000	1000 HRS MINIMUM
RATE GYROSCOPE	UNITED STATES TIME CD 040	±40°/SEC	0.937" DIA X 2-21/64" LG. 4 OZ.	±.0° to ±.2° NONLINEARITY	$1000 - 2000 (INCLUDES PRESSURE CHAMBER FOR 800 PSIA ENVIRON.	14,000 - 15,000 HRS
LINEAR ACCELEROMETER (DC OUTPUT)	SYSTRON DONNER 4311	±.5 g	1.25" DIA X 1.6" LG. 2 OZ.	<±0.1°	$550	40,000 HRS MINIMUM
LINEAR ACCELEROMETER (AC OUTPUT)	KEARFOTT C70-2401	±.5 g	.966" DIA X 1.25" LG. 2 OZ.	BIAS + ZERO STABILITY = 3×10^{-4} g DAY - TO-DAY	$3000 + $1000 FOR EXTERNAL SIGNAL PROCESSING CIRCUITRY	5000 HRS MINIMUM

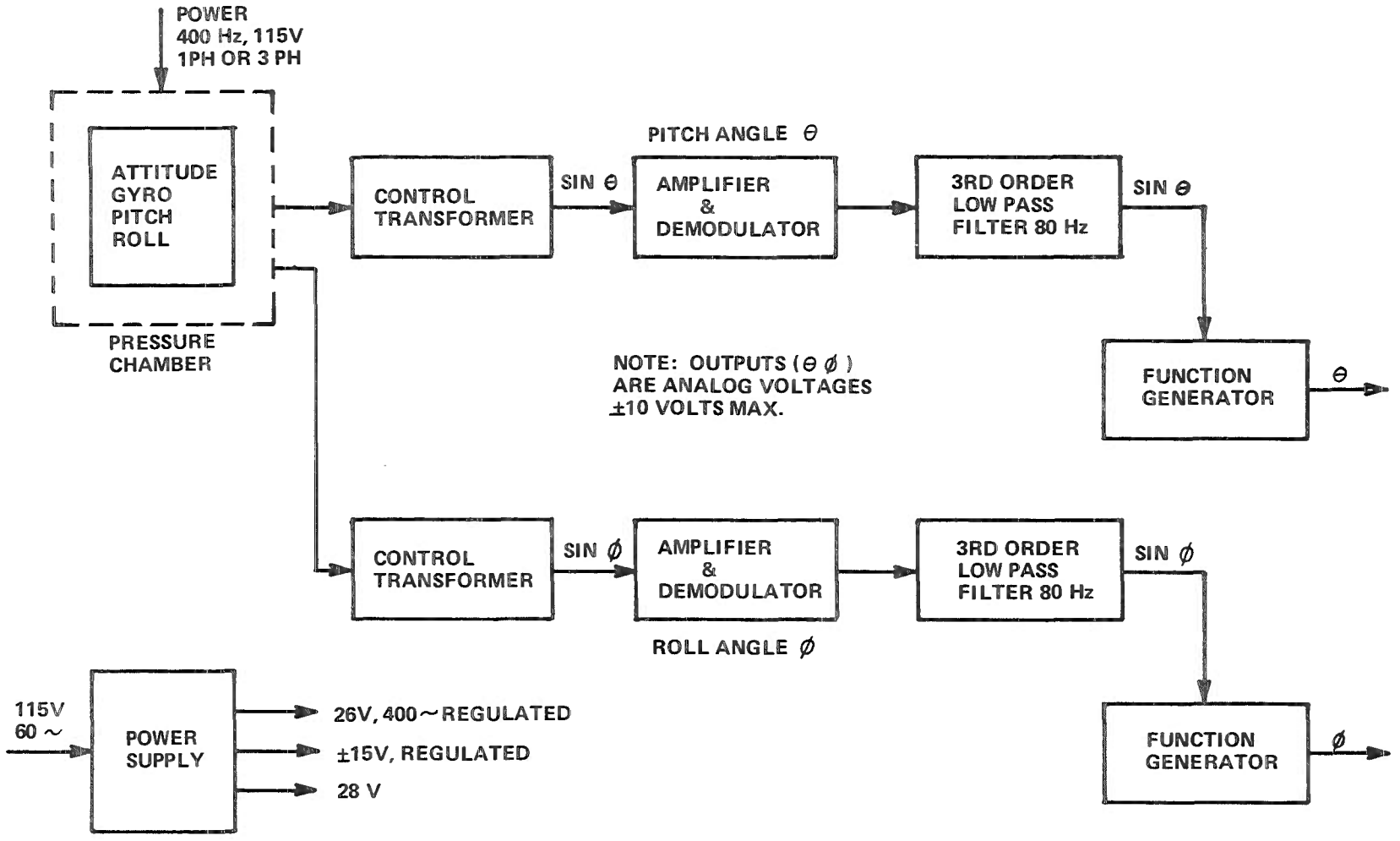

Figure D-1 BLOCK DIAGRAM TYPICAL DISPLACEMENT GYRO SIGNAL PROCESSING ELECTRONICS

3) Typical gyro error of 0.2 to 0.5 degree of pitch angle can be expected. These errors would likely be increased to approximately 0.5 to 0.7 degree due to the electronic circuits which process the gyro output signal.

Rate Gyro Used to Measure Pitch Attitude

Advantages:

1) A rate gyro is a small and very reliable sensor. Its weight and size make it very attractive for insertion in a small sealed pressure chamber.

2) The rate gyro and associated electronics can be easily and accurately calibrated using a standard rate calibration table (such as Inland Controls Model 722).

3) Self-test circuitry is available in rate gyros to provide confidence checks that the entire data channel is operating properly prior to the data run.

4) Calspan Flight Research Department experience has shown that the rate gyro is normally a very reliable and trouble-free instrument.

Disadvantages:

1) The rate gyro requires ac power and ac pickoff excitation. The amplitude and frequency of the excitation signal must be controlled accurately to insure that the desired accuracy of the sensor plus the electronics is obtained (±0.1 degree over range of -10, +20 degrees).

2) The rate signal must be demodulated and filtered prior to recording. Since it is a rate signal, it must be integrated to provide model position information. A post-run digital integration or analog control circuitry is needed to obtain the desired angular measurements.

3) No information can be obtained from the rate gyro about the initial angle of attack of the model. Figure D-2 shows electronic circuits required for the rate gyro sensor.

Linear Accelerometer

A linear accelerometer (Kearfott type C70-2401) is being used successfully by NASA-Langley in their wind tunnel tests. This specific unit requires ac power and ac excitation. The processing circuitry is therefore more complicated than a Systron-Donner Model 4311, for example, which requires only dc power and has a dc output. The required circuitry is shown in

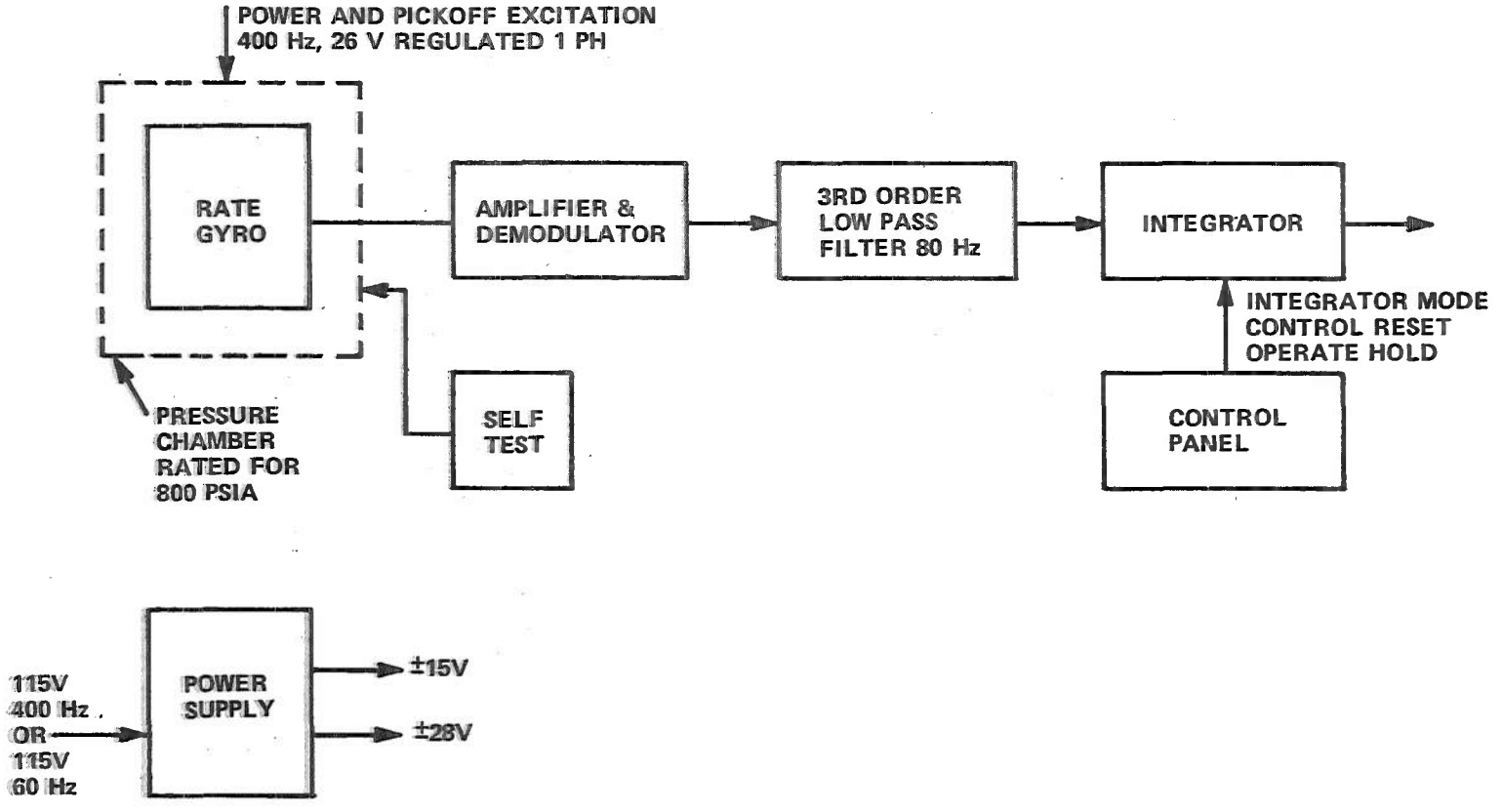

Figure D-2 BLOCK DIAGRAM TYPICAL SIGNAL PROCESSING CIRCUIT USING RATE GYRO SENSOR

Figure D-3. This type of sensor provides good static position information but model vibration may affect its dynamic accuracy.

Combination Rate Gyro and Linear Accelerometer

The most promising device appears to be a combination package of a rate gyro and linear accelerometer. Physically, both units would be enclosed in separate pressure chambers designed to withstand the 800 psia wind tunnel pressure. The two packages would be small enough so that both could be attached to a common mounting plate which would fit into the space available. Since both units would be initially operating at -30°F, which is near their lower temperature limits, it would be advisable to provide a heater and thermal blanket around the entire package to provide protection against thermal transients when the ambient temperature drops to -60°F during the 1/2-second tunnel starting interval. Timex Corporation, manufacturer of the United States Time rate gyros, said a unit used at -30°F could be modified to have the proper damping at that temperature if heaters were not used.

The linear accelerometer would provide the static position information and the rate gyro the dynamic position data. This combination would constitute a complete model position indicator. Since model initial position may be obtained by other methods, such as a manual measurement with an inclinometer, for example, this option should be considered in lieu of an accelerometer if low cost and simplicity are desired.

Figure D-4 shows typical circuitry required. The processing electronics would be outside the chamber at room temperatures. Accurate, reliable and drift-free electronic components such as resistors, capacitors and operational amplifiers are available so that the signal processing electronics should not significantly affect the accuracy of the total signal channel. It is expected that periodic calibration with the sensors at their operating temperatures would satisfy the accuracy requirements stated.

Three basic analog signals would be available: the accelerometer for static data, the rate gyro for dynamic data and a "Kalman" filtered combination which would produce the best overall measurement. The various filter responses could be adjusted to attenuate undesirable frequencies. Notch filters are not shown; however, they would probably be used if necessary to attenuate a particularly dominant undesirable frequency.

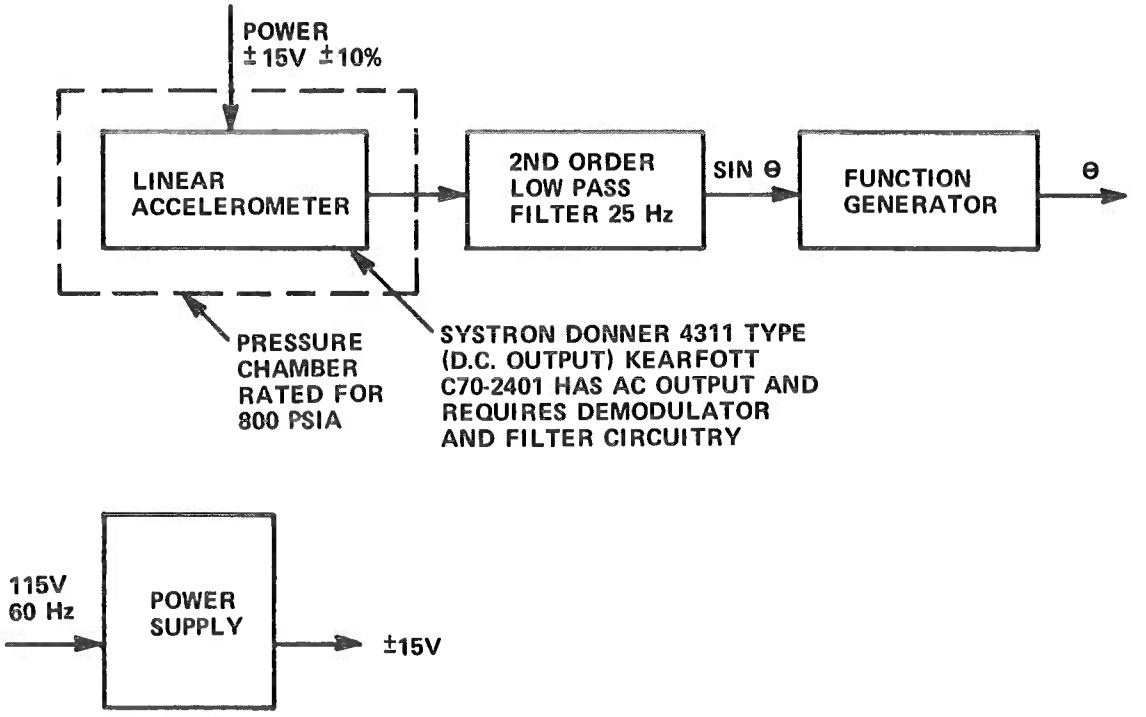

Figure D-3 BLOCK DIAGRAM TYPICAL LINEAR ACCELEROMETER SIGNAL PROCESSING ELECTRONICS

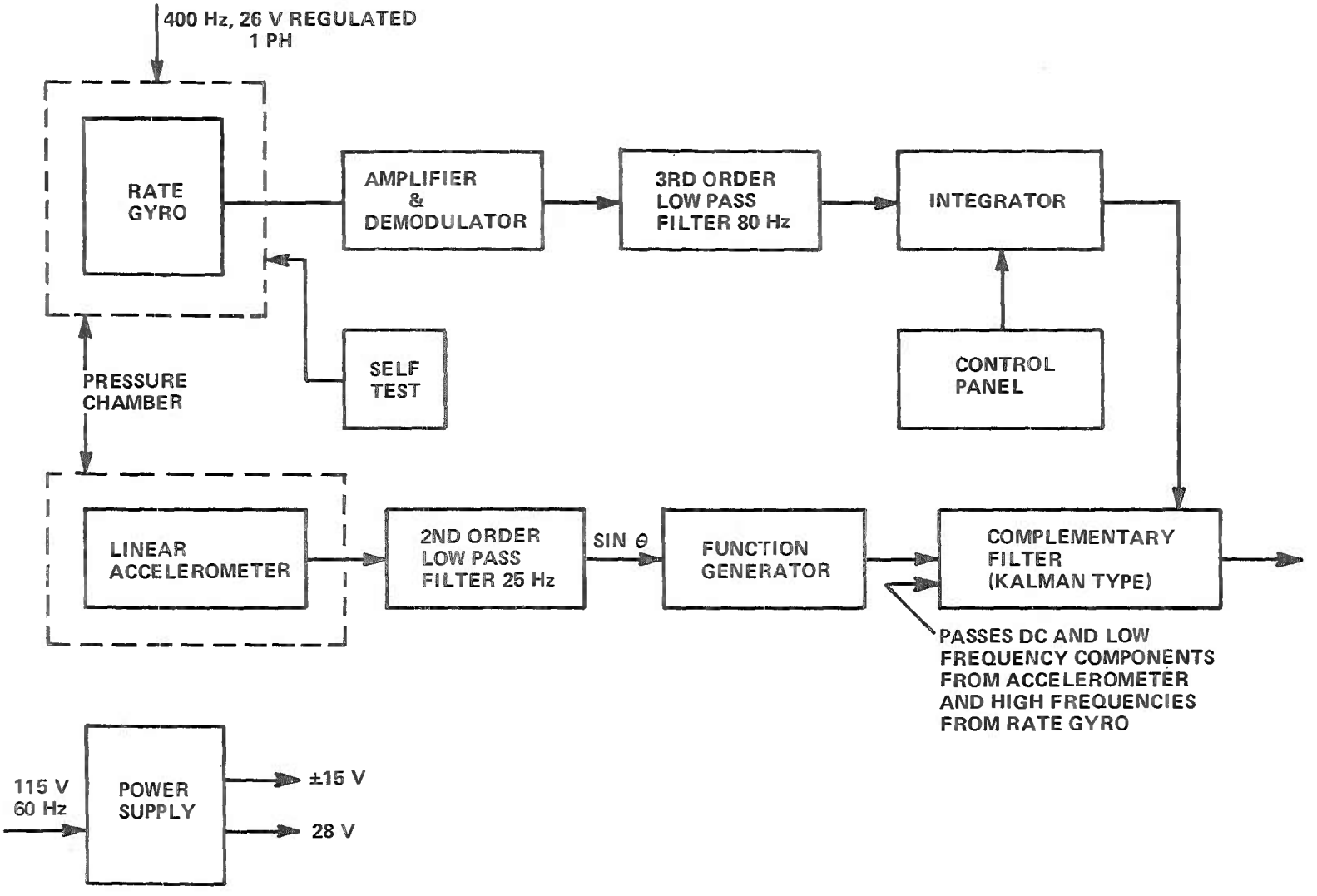

Figure D-4 BLOCK DIAGRAM TYPICAL SIGNAL PROCESSING CIRCUIT COMBINED RATE GYRO AND ACCELEROMETER SENSORS

Appendix E

A LISTING OF THE MEASURED BEAM DEFLECTIONS AND STRAIN GAGE OUTPUTS INCLUDING THE COMPUTED VALUES OF DEFLECTIONS

SUMMARY OF TEST DATA*

RUN NO.	POINT NO.	Y_1 DEFLECTIONS - INCHES	Y_2	Y_3	e_1 BRIDGE OUTPUT - COUNTS	e_2	e_3
1	1	0.0075 0.0078	0.0283 0.0291	0.0545 0.0560	367	89	12
	2	0.0156 0.0159	0.0584 0.0595	0.1132 0.1145	751	188	24
	3	0.0208 0.0210	0.0776 0.0784	0.1504 0.1512	989	248	33
	4	0.0262 0.0264	0.0978 0.0985	0.1894 0.1898	1244	311	41
	5	0.0316 0.0318	0.1177 0.1186	0.2278 0.2287	1500	374	50
	6	0.0266 0.0268	0.0984 0.0991	0.1908 0.1897	1263	309	37
	7	0.0206 0.0210	0.0778 0.0778	0.1506 0.1498	992	243	32
	8	0.0110 0.0110	0.0408 0.0409	0.0796 0.0781	517	129	14
2	1	0.0080 0.0080	0.0263 0.0261	0.0453 0.0447	397	58	-4
	2	0.0152 0.0154	0.0497 0.0501	0.0866 0.0862	760	113	-7
	3	0.0208 0.0211	0.0690 0.0688	0.1192 0.1186	1041	156	-9
	4	0.0250 0.0255	0.0826 0.0831	0.1438 0.1432	1259	188	-11
	5	0.0300 0.0303	0.0986 0.0987	0.1708 0.1703	1496	223	-12
	6	0.0174 0.0178	0.0573 0.0576	0.0993 0.0982	878	128	-11
	7	0.0094 0.0096	0.0310 0.0310	0.0538 0.0529	473	69	-6
3	1	0.0070 0.0070	0.0168 0.0169	0.0270 0.0266	386	-5	0
	2	0.0092 0.0091	0.0222 0.0219	0.0353 0.0343	504	-8	0
	3	0.0154 0.0152	0.0368 0.0367	0.0584 0.0577	841	-12	0
	4	0.0212 0.0212	0.0516 0.0513	0.0818 0.0809	1181	-18	1
	5	0.0270 0.0271	0.0654 0.0657	0.1046 0.1037	1508	-22	2
	6	0.0126 0.0127	0.0311 0.0307	0.0492 0.0485	704	-10	1

SUMMARY OF TEST DATA (Cont.)

RUN NO.	POINT NO.	Y_1	Y_2	Y_3	e_1	e_2	e_3
		DEFLECTIONS - INCHES			BRIDGE OUTPUT - COUNTS		
4	1	-0.0006	0.0228	0.0798	-134	222	104
		-0.0003	0.0226	0.0787			
	2	-0.0048	0.0341	0.1428	-470	433	225
		-0.0046	0.0343	0.1435			
	3	-0.0066	0.0392	0.1688	-608	518	268
		-0.0063	0.0389	0.1680			
	4	-0.0090	0.0458	0.2071	-814	645	342
		-0.0089	0.0458	0.2070			
	5	-0.0116	0.0538	0.2483	-1039	782	417
		-0.0118	0.0531	0.2478			
	6	-0.0140	0.0601	0.2852	-1243	903	485
		-0.0144	0.0593	0.2838			
	7	-0.0102	0.0663	0.2816	-996	862	446
		-0.0102	0.0655	0.2808			
	8	0.0008	0.0800	0.2693	-332	739	342
		0.0010	0.0805	0.2692			
	9	0.0070	0.0773	0.2635	155	560	393
		0.0072	0.0775	0.2648			
	10	0.0118	0.0914	0.2576	352	584	272
		0.0120	0.0916	0.2578			
	11	0.0151	0.0897	0.2539	632	478	302
		0.0155	0.0894	0.2546			
	12	0.0184	0.0866	0.2487	982	347	335
		0.0199	0.0870	0.2499			
	13	0.0213	0.0777	0.1918	1125	216	210
		0.0217	0.0776	0.1932			
5	1	0.0075	0.0278	0.0538	350	86	9
		0.0074	0.0275	0.0524			
	2	0.0151	0.0557	0.1076	711	175	22
		0.0151	0.0559	0.1074			
	3	0.0227	0.0840	0.1620	1071	263	32
		0.0227	0.0842	0.1613			
	4	0.0303	0.1119	0.2158	1431	351	46
		0.0303	0.1124	0.2161			
	5	0.0226	0.0838	0.1616	1065	262	38
		0.0226	0.0837	0.1620			
	6	0.0151	0.0556	0.1075	706	174	26
		0.0150	0.0555	0.1076			
6	1	-0.0081	-0.0299	-0.0573	-378	-95	-13
		-0.0080	-0.0300	-0.0579			
	2	-0.0160	-0.0586	-0.1134	-745	-187	-26
		-0.0158	-0.0590	-0.1142			
	3	-0.0233	-0.0865	-0.1668	-1095	-274	-37
		-0.0233	-0.0867	-0.1674			
	4	-0.0307	-0.1136	-0.2192	-1438	-359	-49
		-0.0306	-0.1137	-0.2196			
	5	-0.0251	-0.0930	-0.1798	-1181	-296	-40
		-0.0251	-0.0936	-0.1807			

SUMMARY OF TEST DATA* (Cont.)

RUN NO.	POINT NO.	Y_1	Y_2	Y_3	e_1	e_2	e_3
		DEFLECTIONS - INCHES			BRIDGE OUTPUT - COUNTS		
7	1	-0.0074	-0.0238	-0.0408	-357	-55	2
		-0.0073	-0.0238	-0.0411			
	2	-0.0122	-0.0396	-0.0688	-604	-091	4
		-0.0122	-0.0399	-0.0697			
	3	-0.0212	-0.0692	-0.1196	-1051	-158	7
		-0.0213	-0.0695	-0.1202			
	4	-0.0254	-0.0830	-0.1438	-1259	-191	9
		-0.0255	-0.0835	-0.1455			
	5	-0.0304	-0.0993	-0.1714	-1502	-228	11
		-0.0304	-0.0997	-0.1724			
	6	-0.0196	-0.0635	-0.1099	-963	-146	7
		-0.0195	-0.0639	-0.1105			
8	1	-0.0074	-0.0182	-0.0285	-411	4	-1
		-0.0074	-0.0182	-0.0290			
	2	-0.0130	-0.0312	-0.0496	-722	8	-2
		-0.0130	-0.0318	-0.0506			
	3	-0.0202	-0.0490	-0.0778	-1121	14	-3
		-0.0202	-0.0491	-0.0781			
	4	-0.0265	-0.0644	-0.1022	-1479	20	-4
		-0.0266	-0.0646	-0.1027			
	5	-0.0126	-0.0304	-0.0482	-693	8	-2
		-0.0125	-0.0304	-0.0485			
9	1	-0.0070	-0.0388	-0.0950	-260	-206	-68
		-0.0069	-0.0389	-0.0943			
	2	-0.0044	-0.0466	-0.1357	-48	-342	-138
		-0.0043	-0.0468	-0.1345			
	3	-0.0022	-0.0526	-0.1682	101	-449	-198
		-0.0026	-0.0537	-0.1686			
	4	0.0010	-0.0616	-0.2152	348	-605	-284
		0.0005	-0.0624	-0.2158			
	5	0.0039	-0.0693	-0.2591	578	-750	-363
		0.0034	-0.0705	-0.2594			
	6	0.0065	-0.0769	-0.2989	788	-881	-437
		0.0061	-0.0777	-0.2993			
	7	0.0102	-0.0870	-0.3550	1084	-1067	-540
		0.0098	-0.0880	-0.3555			
	8	0.0175	-0.0780	-0.3631	1522	-1152	-609
		0.0172	-0.0786	-0.3644			
	9	0.0141	-0.0756	-0.3596	1253	-1049	-635
		0.0139	-0.0765	-0.3602			
	10	0.0068	-0.0718	-0.3532	666	-832	-694
		0.0065	-0.0727	-0.3540			
	11	0.0022	-0.0694	-0.3493	307	-699	-728
		0.0020	-0.0704	-0.3497			
	12	-0.0019	-0.0674	-0.3454	-33	-572	-764
		-0.0022	-0.0681	-0.3461			

SUMMARY OF TEST DATA* (Cont.)

RUN NO.	POINT NO.	Y_1	Y_2	Y_3	e_1	e_2	e_3
		DEFLECTIONS - INCHES			BRIDGE OUTPUT - COUNTS		
9 (Cont.)	13	-0.0044 -0.0045	-0.0660 -0.0666	-0.3432 -0.3439	-217	-502	-784
	14	-0.0094 -0.0095	-0.0638 -0.0639	-0.3390 -0.3390	-616	-353	-823
	15	-0.0078 -0.0076	-0.0600 -0.0598	-0.3452 -0.3438	-532	-356	-866
	16	-0.0069 -0.0069	-0.0646 -0.0643	-0.3711 -0.3710	-472	-416	-927
	17	-0.0046 -0.0044	-0.0575 -0.0572	-0.3747 -0.3746	-372	-404	-988
10	1 ($\theta = 0^o$)	0.0101 0.0093	0.0974 0.0958	0.4538 0.4528	456	658	983
	2 ($\theta = 2.75^o$)	0.0089 0.0074	0.1010 0.0988	0.4404 0.4380	254	736	886
	3 ($\theta = 1.4^o$)	0.0094 0.0081	0.0994 0.0969	0.4467 0.4444	334	701	932
	4 ($\theta = 0^o$)	0.0097 0.0087	0.0966 0.0949	0.4528 0.4517	418	664	983
	5 ($\theta = 0^o$)	0.0180 0.0172	0.1052 0.1035	0.3801 0.3783	830	556	675
	6 ($\theta = 1.4^o$)	0.0176 0.0165	0.1058 0.1045	0.3748 0.3744	764	582	646
	7 ($\theta = 2.75^o$)	0.0170 0.0158	0.1098 0.1069	0.3659 0.3654	663	627	583
	8 ($\theta = 0^o$)	0.0181 0.0171	0.1045 0.1034	0.3806 0.3788	828	556	677
11	1	0.0354 0.0344	0.2644 0.2630	0.8725 0.8710	1235	1658	1294
	2	0.0418 0.0414	0.2700 0.2690	0.7404 0.7405	1461	1570	774
	3	0.0300 0.0295	0.2183 0.2171	0.5832 0.5828	858	1365	540
	4	0.0346 0.0341	0.1874 0.1866	0.4522 0.4517	1308	968	330
	5	0.0242 0.0238	0.1560 0.1552	0.3986 0.3986	787	912	334
	6	0.0268 0.0265	0.1500 0.1493	0.3309 0.3301	930	799	136
	7	0.0214 0.0211	0.1155 0.1149	0.2727 0.2721	801	595	180
	8	0.0243 0.0242	0.1016 0.1013	0.2044 0.2038	1065	393	55
	9	0.0138 0.0139	0.0522 0.0518	0.1006 0.1008	655	164	25
	10	0.0063 0.0063	0.0232 0.0233	0.0454 0.0432	294	73	3

SUMMARY OF TEST DATA* (Cont.)

RUN NO.	POINT NO.	Y_1	Y_2	Y_3	e_1	e_2	e_3
		DEFLECTIONS - INCHES			BRIDGE OUTPUT - COUNTS		
12 (-8.5°F)	1	0.0075 0.0073	0.0278 0.0275	0.0538 0.0557	350	87	22
	2	0.0151 0.0150	0.0557 0.0558	0.1076 0.1078	707	176	24
	3	0.0227 0.0225	0.0840 0.0837	0.1620 0.1619	1061	264	37
	4	0.0303 0.0301	0.1119 0.1118	0.2158 0.2159	1419	352	48
	5	0.0226 0.0225	0.0838 0.0837	0.1616 0.1616	1060	264	36
	6	0.0151 0.0149	0.0556 0.0555	0.1075 0.1072	703	175	24
	7	0.0075 0.0073	0.0278 0.0272	0.0538 0.0553	345	87	22
13 (-40.0°F)	1	0.0075 0.0075	0.0278 0.0279	0.0538 0.0536	353	88	11
	2	0.0151 0.0151	0.0557 0.0560	0.1076 0.1077	710	176	23
	3	0.0227 0.0227	0.0840 0.0841	0.1620 0.1617	1068	264	34
	4	0.0303 0.0302	0.1119 0.1121	0.2158 0.2161	1425	352	47
	5	0.0226 0.0226	0.0838 0.0839	0.1616 0.1617	1065	264	35
	6	0.0151 0.0150	0.0556 0.0558	0.1075 0.1074	706	176	23
	7	0.0075 0.0074	0.0278 0.0276	0.0538 0.0531	350	87	11

*CALCULATED DEFLECTION IS THE SECOND ONE LISTED